Master's Thesis

Heparin-Polymersome Conjugates to Fool Plasmodium Merozoites

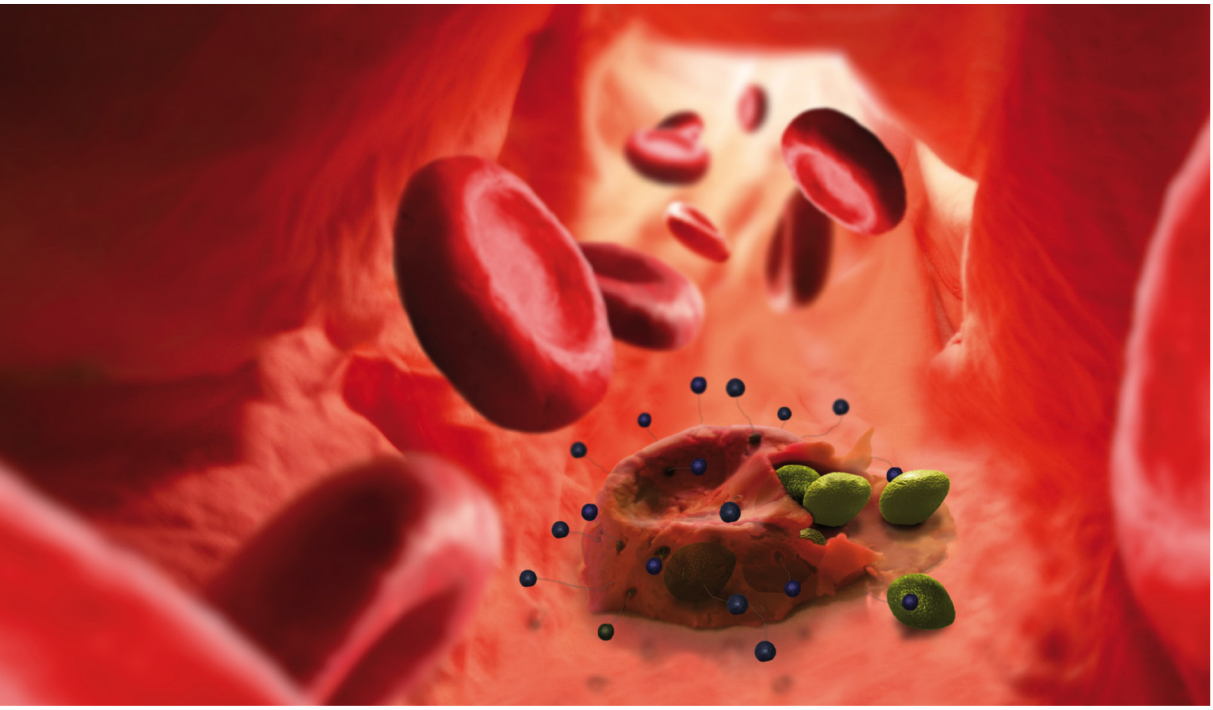

Adrian Najer, Student of the SNI, Basel, Switzerland

July 30, 2011

UNI
BASEL

Abstract

Here, a new nanotechnological approach to produce an antimalarial agent is presented. The concept of this project was to capture *Plasmodium* merozoites by using polymersomes that mimic the surface of the erythrocyte, in particular the important features that mediate the initial contact between merozoites and erythrocytes, which are thought to be heparin-like molecules. Additional targeting of these heparin-polymersome conjugates at infected erythrocytes (IEs) would increase drug efficacy. Two different conjugation approaches to prepare these heparin-polymersomes were tested. One based on linker chemistry leading to a stable, UV detectable, biocompatible bis-aryl hydrazone bond. For this purpose, a readily-accessible primary amino group was first attached to heparin. The other approach was a direct reductive amination between the reducing end of heparin and the secondary amines on the polymersome surfaces. Both pathways led to unclear results. Either it was a detection problem or the conjugations did not work properly. Initial *in vitro* tests for antimalarial activity of heparin-polymersome conjugates failed to show invasion inhibition. Even heparin at 100 μg/ml did not inhibit erythrocyte invasion by *Plasmodium* merozoites as reported. In future, other conjugation and analysis methods should be evaluated and *in vitro* tests have to be optimized.

Abbreviations

2,6-DAP = 2,6-diaminopyridine
2-HyPy = 2-hydrazino pyridine
4-FB = 4-formylbenzamide
4-NB = 4-nitrobenzaldehyde
AbHep = anti-heparin antibody
AbHepOG488 = anti-heparin antibody Oregon Green 488 conjugate
AB-OH = PDMS-*b*-PMOXA diblock copolymer with hydroxyl terminus
AB-NH = PDMS-*b*-PMOXA diblock copolymer with piperazyl terminus
AMA1 = apical membrane antigen 1
CSP = circumsporozoite surface protein
DAPH = 2,6-diaminopyridinyl heparin full-length
DAPH-LMW = 2,6-diaminopyridinyl heparin low molecular weight
ddH_2O = double distilled water
FCS = fluorescence correlation spectroscopy
GIA = growth inhibition assay
HyNic = 6-hydrazino-nicotinamide
IE = Plasmodium infected erythrocyte
MPS = major phagocytic system
MSP1/3/6/7 = major surface proteins of the families 1/3/6/7
MW = molecular weight
MWCO = molecular weight cut-off
NHS = N-hydroxy succinimide
OG488 = Oregon Green 488
PDMS = poly(dimethylsiloxane)
PEG_4-PFB = poly(ethylene glycol)$_4$-pentafluorophenyl ester 4-formylbenzoate
PfEMP1 = Plasmodium falciparum erythrocyte membrane protein 1
PMOXA = poly(2-methyloxazoline)
ProtOG488 = protamine Oregon Green 488 conjugate
SRB = sulforhodamine B
Sulfo-S-4FB = sulfo-succinimidyl-4-formylbenzoate
Sulfo-S-HyNic = sulfo-succinimidyl-6-hydrazinonicotinate acetone hydrazone
TEM = transmission electron microscopy
V-4FB = 4-FB modified polymersomes using Sulfo-S-4FB linker
V-NH = unmodified polymersomes with 5% AB-NH
V-PEG4FB = PEG-4-FB modified polymersomes using PEG_4-PFB linker
V-SRB = unmodified polymersomes with 100% AB-OH and 0.6 mM SRB incorperated

Contents

1 Introduction

Malaria remains a leading disease in developing countries, causing approximately 800,000 deaths annually [1]. There is still no fully satisfying vaccine on the way to the market and multiple drug resistances has emerged, limiting the use of most antimalarials. Important factors for the high mortality related to malaria are problems in distribution and financing of the antimalarials. At the moment, artemisinin-based combination therapies are very effective for malaria and are the recommended first-line treatment in endemic regions, but drug resistance to artesunate, a drug of the artemisinin-group, was suspected recently [2]. Therefore, research into potential new drugs is needed, even whilst an eradication agenda is in process [1,3]. The currently existing and future drug strategies against malaria are listed in Ref. [3]. No drugs targeting merozoite invasion or egress are known to date.

Nanotechnology, a fast growing technological field, should also greatly affect future medicine favourably in this regard. Nanocarriers can take a drug to a specific target, increase drug efficacy, and reduce toxic side effects [4]. New nanosized systems may provide improvements in current antimalarials, or unique solutions, or at least new research tools for the design of new antimalarial treatments. In this work here, the first steps to create a nanotechnological solution to inhibit merozoites, the free parasite blood stage, from invading new erythrocytes have been completed. The current knowledge on the life cycle of *Plasmodium*, current intervention strategies, the molecular mechanism of erythrocyte invasion by merozoites, and the pathogenesis of malaria are summarized in the following. Then, the impact of nanotechnology on medicine, heparin-nanoparticles, polymersomes as a medical tool, and the already tested possible nanotechnological contributions to antimalarial treatment will be discussed in the sub-introductory sections. Finally, the general concept of this work is described and the details on the achievement of these goals are presented.

1.1 Malaria

Malaria is an infectious disease caused by the apicomplexan organism *Plasmodium* which is transmitted by *Anopheles* mosquito species. *Plasmodium* has an extraordinarily complex life cycle. The five species *P. falciparum*, *P. vivax*, *P. ovale*, *P. malariae*, and *P. knowlesi* can infect humans and cause this disease, whereas *P. falciparum* is responsible for most severe infections. Only the topics of malaria which are relevant to this work are discussed in this introduction.

1.1.1 Life Cycle and Current Intervention Strategies

Here, only part of the complex life cycle is summarized. A bite by an *Plasmodium* infected *Anopheles* mosquito delivers sporozoites into the human blood stream. This form of the parasite can pass through Kupffer cells in the liver and then exclusively invade the hepatocytes. Inside an hepatocyte a single sporozoite produces thousands of merozoites. This form can now infect erythrocytes. Inside an erythrocyte the merozoite undergoes several changes. First, it becomes a round trophozoite (ring stage) located within a parasitophorous vacuole in the erythrocyte. After the trophozoite has grown,

it undergoes schizogonic division. Afterwards the schizont bursts and releases about 16 to 30 merozoites, which infect new erythrocytes [5]. This asexual blood stage life cycle is repeated continuously. The blood stage form of *Plasmodium* is responsible for the pathogenesis of the disease.

Currently, the only vaccine in phase III trials is RTS,S, a pre-erythrocytic malaria vaccine based on the circumsporozoite surface protein (CSP) of *P. falciparum*. Protection ranging from 35% - 53% was demonstrated [6]. On the other hand, there are great efforts being made to develop a vaccine for blood stage parasites. The two antigens, major surface protein 1 (MSP1) and apical membrane antigen 1 (AMA1) on the merozoite surface, are the main candidates for an anti-blood stage vaccine [7]. One promising reason for the use of MSP1 is the finding that antibodies specific to MSP1-19, a proteolytically processed fragment of MSP1, are the major component of protection in many *P. falciparum*-immune humans [8]. But there is also some evidence that the immune reaction to MSP1-33, another proteolytically processed fragment of MSP1, is required for protection as well. Antigenic diversity is perhaps the biggest challenge for a blood stage malaria vaccine [9]. Most important antigens show polymorphism, only some subregions are less diverse or conserved. It will be very difficult and time-consuming to combine several allelic forms of one antigen in a single vaccine.
In conclusion, the vaccine with the highest efficacy will most probably be a combination of a pre-erythrocytic vaccine such as RTS,S and an effective blood stage vaccine. Such a trial was carried out in a recent study and showed 50% efficacy with a virosome-formulated AMA1 and CSP combination [10]. But a vaccine should also reduce transmission if it is to eradicate malaria [1]. Therefore, a reduction in clinical illness is desirable, but not the only challenge. The fact that a reduction in parasites in the blood stream leads to a decrease in the number of gametocytes provides hope that, with an efficient vaccine, also transmission will be reduced [9]. There is also development of transmission blocking vaccines.

On the antimalarial side, there are several different, very effective drug combinations known, although resistance is emerging. Growth inhibition assay (GIA) is a standard method to test the efficiency of antimalarials *in vitro*. Artemisinin and its derivatives (artesunate, artemether, dihydroartemisinin), the recommended first-line treatment drugs, have shown IC_{50} (molar drug concentration required to inhibit parasite growth by 50%) for drug concentrations between 0.006 and 5 nM [11].

1.1.2 Early Events of Erythrocyte Invasion by *P. Falciparum* Merozoites

Invasion of erythrocytes by merozoites is a multistep process in which many specific receptor-ligand interactions are involved. A nice, high-resolution movie of an invasion process and description of core cellular and molecular steps of invasion and their hierarchy are visible in Ref. [12]. In this section some interactions and processing events, important in the early invasion steps, are discussed in the order as they occur during invasion. The following explanations are based, in general, on a review by Alan F. Cowman and Brendan S. Crabb [5]. If not indicated otherwise, the information was gathered from this review. Figure 1 shows a single merozoite with its most important organelles and cell structures and the multistep invasion process is schematically represented. The molecular basis of the early processes (A,B) is discussed in detail below.

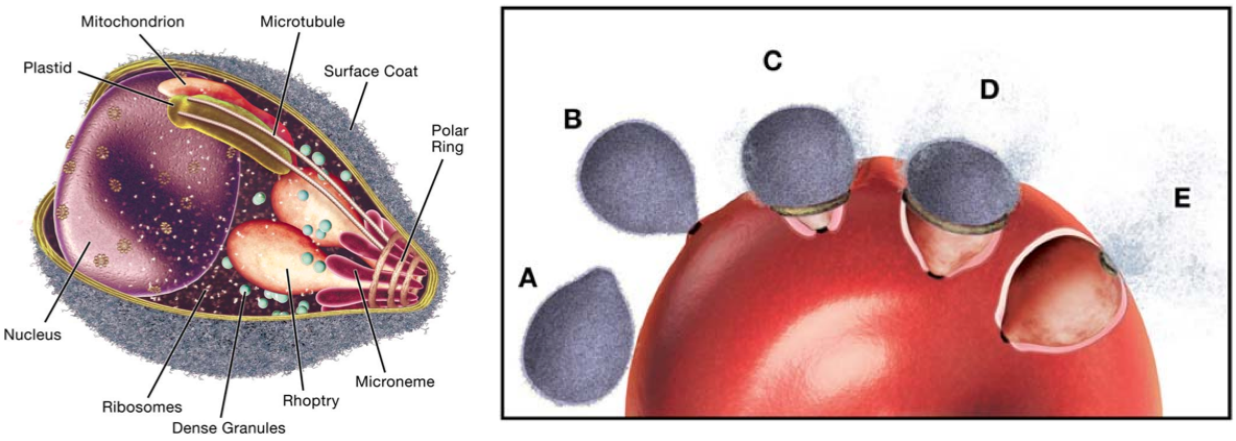

Figure 1: Left: Schematic picture of a merozoite with its most important organelles and cellular structures. Right: Schematic representation of the invasion of an erythrocyte by a merozoite. A) Initial contact, B) Reorientation and tight junction formation, C)+D) Tight junction movement from apical to posterior pole, E) Adhesive proteins at junction proteolytically removed [5].

The proteins responsible for the initial, low-affinity contact (Fig. 1A) between erythrocytes and merozoites are still not completely determined. One reasonable candidate is MSP1, which is the most abundant surface protein on merozoites. At the moment, the crystal structure of the MSP1 complex is not determined, which is one problem related to why its role cannot be clearly defined [13]. On the erythrocytic site, one possible ligand for the initial contact is thought to be heparan sulfate proteoglycan, which is structurally very similar to heparin [14, 15]. Others showed that MSP1-19 binds to band 3 proteins on erythrocytes, probably with MSP9 as co-receptor [13]. Other possible candidates for the initial contact are peripheral proteins on merozoits, which can be classified into three groups: MSP-3/-6 group, MSP-7 family, and the SERA protease family. It is still not known which of these candidates are essential for initial recognition and contact, no final conclusions can be drawn at the moment.

To understand the suggested role of MSP1 in early invasion events, the processing steps for this protein are discussed in more detail (Fig. 2). MSP1 is a glycosylphosphatidylinositol (GPI)-anchored membrane protein. The first processing step is necessary to produce mature merozoites before they are released from the infected erythrocyte (IE). This means that this happens before all of the invasion steps (Fig. 1 A-E). The peripheral proteins MSP6 and MSP7-33 are secreted into the intraerythrocytic parasitophorous vacuole (PV), where they can form a complex with MSP1 (MSP1/6/7 complex). Just before the egress of the merozoites from the erythrocyte, subtilisin-like proteases 1 (PfSUB1) are released from exonemes into the PV lumen. PfSUB1 is responsible for the primary processing on the MSP1/6/7-complex, which leads to the mature merozoites with the MSP1-30/MSP1-38/MSP1-42/MSP1-83/MSP6-36/MSP7-22/19 complex on their surfaces [16]. These MSP-fragments are held together by non-covalent interactions [13]. After the erythrocyte bursts, the merozoites reach the blood stream, where they attach to new erythrocytes (Fig. 1A) probably via their mature MSP1/6/7 complex.

After this initial contact between merozoite and erythrocyte is established, the content of the mi-

cronemes (secretory organelles) is expelled at the apical end of the merozoite. PfSUB2 which is also located in the micronemes, is released and migrates, as membrane bound protease, along the merozoite surface and performs the secondary processing on the MSP1/6/7 complex [17] (Fig. 2). The MSP1-19 is the only fragment of the whole MSP1/6/7 complex that remains on the merozoite surface during invasion, it contains two epidermal growth factor (EGF)-like domains. But radical changes in these EGF-like domains does not inhibit invasion; therefore, the definitive function of MSP1-19 has still to be proven [18].

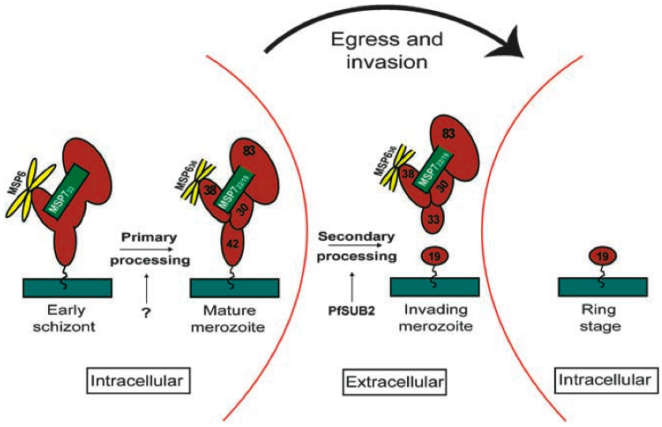

Figure 2: Proteolytic processing of the MSP1/6/7 complex. Primary processing is carried out by PfSUB1 just before egress of the merozoites from the erythrocyte. Secondary processing occurs extracellularly by the membrane bound protease PfSUB2 [16].

Heparin and other sulfated glycosaminoglycans have already been successfully tested for their antimalarial activity *in vitro* [15, 19–22]. But some initial *in vivo* experiments with monkeys and humans have not shown any benefit upon heparin treatment [23, 24]. Problems for the usage of such a compound for antimalarial treatments are: the anticoagulation properties of heparin, the high dosage needed, short plasma half-life of about 1 hour, and the need for parenteral administration [22].

In the beginning it was claimed that non-specific interactions with the negative charges on sulfated glycosaminoglycans gave rise to the inhibition of invasion and endothelial adhesion of IEs [20]. But later it was found that specific interactions of sulfated glycosaminoglycans with MSP1 are responsible for invasion inhibition [15, 21]. To test if entry of heparin into IEs is necessary for invasion inhibition, heparin was coupled to agarose beads [21]. It was found that this formulation also inhibits invasion, but higher doses were needed. Recently, it was shown that heparin-like molecules block early and essential events in erythrocyte invasion by merozoites. Specific interactions between heparin-like molecules and MSP1-42, MSP1-33, but not with MSP1-19, were demonstrated [15]. In a GIA with 1% parasitemia and 1% hematocrit a heparin concentration of about 1.4 μM was necessary for IC_{50} and in the case of the heparin-analog K5 from the capsule of *Escherichia coli*, about 0.5 μM. These concentrations are higher by about a factor of 1000 than for artemisinins [11]. Because K5 is non-immunogenic [25] and has no anticoagulation properties, it is a possible candidate for the design of a new drug formulation for malaria [15].

1.1.3 Pathogenesis of Malaria

After the parasite has entered an erythrocyte, it changes the transcription of proteins dramatically. Several new proteins are expressed and transported to the erythrocyte membrane. One of these proteins is *P. falciparum* erythrocyte membrane protein 1 (PfEMP1). The following section is based on several review articles covering antigenic variation in *P. falciparum* [26–28], and its relation to the pathogenesis of the disease [29–31]. The clonally variable surface antigens PfEMP1 are transcribed and subsequently transported to the membrane of the infected erythrocytes (IEs) during 20 to 30 hours post-invasion. These variant PfEMP1s are encoded by a multigene family named *var* genes. Approximately 60 different *var* genes are located in the genome of *P. falciparum*, but only one specific allele is transcribed in one IE at a time. PfEMP1s bind to knob-associated His-rich proteins (KAHRPs) with their cytoplasmatic domain. KAHRPs are soluble proteins that deposit and self-assemble at the cytoplasmic face of the erythrocyte membrane from about 16 hours post-invasion, where they form small protrusions called knobs (approx. 100 nm diameter) [26]. On the title page these knobs are drawn as black dots on the IE.

Because IEs present such parasite proteins (mainly PfEMP1) on their surfaces after about 24 hours post-invasion, these proteins would be major targets for an immune response to clear the blood of IEs. But the parasite has evolved two survival strategies for IEs. First, the parasite is able to switch between the *var* genes in a controlled way. Secondly, the PfEMP1 proteins on IEs can establish several interactions with different receptors on many host cells. Therefore, IEs no longer circulate freely in the blood stream and clearance of the IEs by phagocytic cells in the spleen can be avoided. With these two strategies the parasite changes the antigenic and the functional properties of IEs. Thus, evasion from the immune response can also change the severity of the disease.

Now, the focus is the link between the PfEMP1 function and the severity of the disease. PfEMP1 is responsible for several interactions between IEs and different host cells in various organs including heart, lung, brain, liver, kidney, subcutaneous tissue and placenta [29]. These interactions are probably the main causes for the pathogenesis of the disease. Depending on which type of *var* gene was expressed, IEs can bind to other cell types.

In more detail, the DBL and CDIR domains of PfEMP1 are responsible for the different binding properties. Several receptors for PfEMP1 on host cells were found and related to specific IE host cell interactions. Some of these receptors are: thrombospondin (TSP), CD36, intercellular adhesion molecule 1 (ICAM-1), vascular cell adhesion molecule, E-selectin, chondroitin sulphate A (CSA), CD31, complement receptor 1 (CR1), heparan sulfate (HS) and hyaluronic acid (HA) [29, 30]. Binding of IEs to CD36 leads to sequestration in microvasculature (Fig. 3 right), autoagglutination and dysregulation of dendritic cells. CSA is present on the surface of placental syncytiotrophoblasts, and binding with IEs presenting PfEMP1 expressed by the *var2CSA* gene on its surface causes placental malaria. CR1 on uninfected erythrocytes interacts with IEs, which leads to rosettes (Fig. 3 left). The ligand for HS on IEs is PfEMP1, and a specific variant of PfEMP1 can also bind heparin, the highly sulfated form of HS [32]. Furthermore, it was proposed that UpsA *var* genes and UpsC *var* genes are

associated with severe or mild infections, respectively [31].

The role of adhesion of IEs to human cells and the corresponding therapeutic implications were reviewed in Ref. [32]. The mortality for severe malaria is 15 - 20% despite treatment with effective antimalarials, even in well-equipped hospitals. Therefore, adjunctive therapies to treat severe malaria are needed [32]. These adjunctive drugs should be able to reverse adhesion of IEs to human cells (Fig. 3). Heparin was one candidate which could reverse rosetting in a subset of parasite isolates and cytoadherence of IEs to endothelial cells was inhibited [20, 33]. General information about heparin and some therapeutic effects are presented in section 1.2.1.

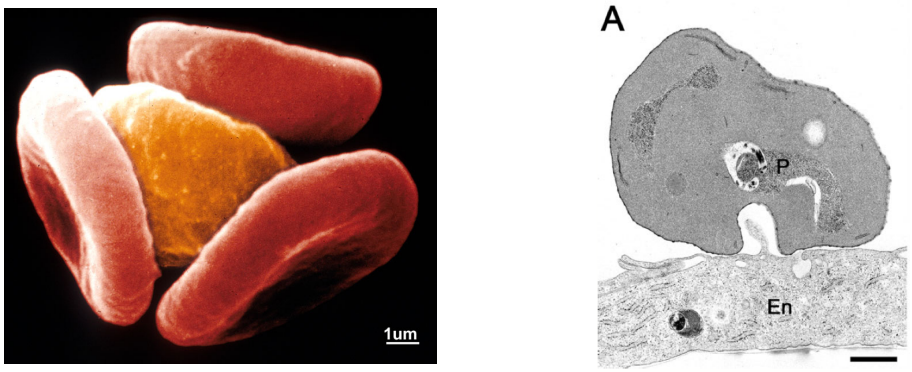

Figure 3: Left: Scanning electron micrograph of an infected erythrocyte forming a rosette with three uninfected erythrocytes [34]. Right: Transmission electron micrograph of the infected erythrocyte-endothelium interaction, scale bar 1 µm [35].

Because of the high antigenic variation of PfEMP1, vaccines based on this protein only could stop one particular form of the disease, e.g. placental malaria. If the parasite inside an IE switches expression from the *var2CSA* gene to another, the protection is lost. This means that the IEs can no longer bind to placental CSA, and therefore this would eliminate placental malaria, but the expression of another PfEMP1 can lead to other severe problems. Another problem is the high diversity between *var* genes of different strains [27, 28].

1.2 Nanotechnology in Medicine

Nanotechnology provides the possibility of constructing nanosized systems with unique properties. These newly designed nanosystems can be applied to medical purposes. They will have great impact on disease diagnosis, treatment, and prevention [4]. One topic of huge interest is drug delivery. Conventional drug administration distributes the drug throughout the entire body. Undesired side effects can appear and high drug doses are typically needed to achieve the pharmaceutical effect in the desired tissue in the end. Therefore, nanocarriers were designed to encapsulate the drug and protect it from the environment. Furthermore, these loaded drug containers can be targeted to a desired tissue and release the drug only at a certain site. Drugs with low bioavailability can be incorporated into a carrier to enhance their bioavailability [36].

For this theory to be applied to the treatment of humans, the nanosystems must fulfil some impor-

tant criteria. These criteria are dependent on the desired site of action of the nanocarrier. First, the nanoparticle should be smaller than 200 nm or it should be deformable to bypass the human splenic filtration process [37]. Second, the surface of the nanocarrier has to be protein repellent and non-immunogenic in order to avoid their clearance by the mononuclear phagocytic system (MPS) [38]. Thirdly, the carrier system has to be stable and impermeable so that the drug does not leak out of the container. Fourthly, if targeting to a specific tissue is desired the ligands have to be stably attached to the carrier [39]. Obviously, the nanocarrier has to be biocompatible as well.

Different nanosystems including carbon nanotubes, nanomachines, nanofibers, self-assembling polymeric nanoconstructs, nanomembranes, and nano-sized silicon chips were proposed for such applications [4]. Because of the improved stability of artificial nanocarriers compared to liposomes, they should be more stable in gastrointestinal fluid, and the oral administration of therapeutic agents with low bioavailability encapsulated in nanospheres should be possible [40].

Nanotechnological solutions to treat infectious diseases are also under development [41]. The treatment of severe infections often requires the use of highly toxic drugs which cause serious side effects. The encapsulation and targeted delivery of these drugs would probably overcome this disadvantage [41]. There is one such drug formulation approved for the treatment of leishmaniasis (AmBisome®) [42]. It is a liposomal formulation of amphotericin B. The human host cells of *Leishmania* are macrophages. Therefore, a passive targeting strategy is used. The liposomes need no special features on the surface, because here the uptake by macrophages is desired in order to release the drug inside the macrophage and kill the parasite in the host. Generally, if the nanosystem is not to be taken up by cells of the MPS, it needs special features. In order to maintain these long-circulating nanoparticles in the blood stream one could mimic the strategies of the erythrocytes or of pathogens [37]. One of these strategies is the functionalization of nanoparticles with the sulfated glycosaminoglycan heparin [43]. As a candidate for a suitable delivery system polymeric vesicles, called polymersomes, are of great interest [44].

1.2.1 Heparin Nanoparticles

The highly sulfated linear polysaccharide heparin (MW = 18 kDa) consists of an average of 60 monomers (MW = 300 Da) per chain and low molecular weight heparin (LMWH, MW = 5 kDa) of an average of 17 monomers per chain. The most common residues in heparin are 2-O-sulfo-α-L-iduronic acid (IdoA(2S)) and 2-deoxy-2-sulfamido-α-D-glucopyranosyl-6-O-sulfate (GlcNS(6S)). These two residues make up 75% of heparin from porcine intestinal mucosa [45]. The chemical structure of such a dimer is shown in the appendix (Fig. 28). The abbreviations 2S or 6S in the brackets indicate the positions that are sulfated in each residue.

Heparin is known as an anticoagulation drug. The basis for its anticoagulant activity is the complex built with antithrombin III via the negative charges on heparin [46]. A specific pentasaccharide is necessary for this activity, but only about 22% of heparin and approx. 16% of LMWH contain this sequence [47]. Heparin (MWCO = 15 kDa) as an anticoagulation drug is used in the concentration range of 0.8 to 3.2 μM (12 μg/ml) during surgery or clinical anticoagulation therapy [48].

Interestingly, artificial sulfated peptides can be constructed to bind heparin-binding proteins, therefore mimicking the effect of heparin [49, 50]. Because the anticoagulation property of heparin is not important for this work, no detailed information about the mechanism is given here. This information can be found elsewhere [47]. Some other important effects of heparin will now be described.

Heparin has a short plasma half-life of approximately 90 minutes [51]. Heparin is given parenterally by intravenous or subcutaneous injection. The low bioavailability could be overcome by the formulation of heparin with a delivery agent [52, 53], and oral administration of heparin becomes possible.

On the other hand, heparin is coupled to nanoparticles to increase the circulation time of the particles in the blood stream [37]. Heparin-coated nanoparticles exhibited an initial phase of elimination from the blood with a half-life of 5 h, the remaining heparin nanoparticles circulated for about 48 h [43]. The same nanoparticles without the heparin had a half-life of only 3 min. Generally, nanodevices are functionalized with glycosaminoglycans to mimic cell surfaces, in order to evade the immune system [54]. Furthermore, heparin inhibits the complement system [55]. Several methods to construct heparin-nanoparticle conjugates, and applications of such conjugates are reviewed in Ref. [54]. The synthesis, properties, and applications of polysaccharide-containing block copolymers is summarized in Ref. [56].

In case of infectious diseases, glycosaminoglycans also play an important role [57]. In the case of heparin, it was found that it is the receptor on host cells for many viruses [58] and as we have seen, probably for the malaria parasite [15]. Heparin has also shown some effect in reversing rosettes in severe malaria [33]. Heparin has even already used to treat severe malaria, but these treatments were stopped because serious side effects, such as intracranial bleedings, occurred [33]. This happens because of the anticoagulation properties of heparin. Modified heparin with lowered anticoagulation effect can possibly become an adjunctive treatment for severe malaria [33].

1.2.2 Polymersomes for Medical Purposes

Amphiphilic block copolymers, containing at least one hydrophilic (A) and one hydrophobic block (B), will spontaneously self-assemble into different ordered structures such as spherical micelles, worm-like micelles, and closed bi- or multilayer structures [44, 59]. By fine-tuning parameters such as hydrophilic-hydrophobic nature and ratio, as well as physical parameters, it is possible to get a desired structure. Compared to liposomes, polymersomes are more stable and tough and offer numerous possibilities of tailoring physical, chemical, and biological properties by variation of block lengths, chemical structure, and conjugation with biomolecules [59, 60]. Not only lipid-analog diblock copolymers (AB) are useful, but also triblock copolymers (ABA or ABC) can be designed to yield desired structures.

In terms of using polymersomes for medical purposes such as drug delivery, their stability is too high to release the drug at a desired site [61]. But because of the unique tailoring possibilities of polymersomes, stimuli-responsive polymers can be designed [61–63]. Another possibility is the incorporation of channel proteins into the polymer membranes in order to achieve selective permeability [64].

The polymersomes should also fulfil the criteria for use as nanoparticles in medical applications as listed above.

Polymersomes made of poly-(dimethylsiloxane)-poly(2-methyloxazoline) (PDMS-*b*-PMOXA) diblock copolymers should be a suitable carrier system [39, 65–67]. It has been shown that PMOXA is protein repellent [68, 69]. Furthermore, PDMS is biocompatible [70]. Stealth properties were obtained by surface modification of liposomes with PMOXA, which led to the same long circulation and low hepatosplenic uptake in rats as for very well known polyethylene glycol (PEG)-modified liposomes [38, 68]. For purely polymeric PMOXA-*b*-PDMS-*b*-PMOXA vesicles, stealth properties have also been described [39]. Polymersomes made of amphiphilic triblock copolymers (ABA, PMOXA-*b*-PDMS-*b*-PMOXA) showed no toxic effects in *in vitro* experiments [39, 66]. Furthermore, these polymersomes made of the same triblock copolymer are non-immunogenic, immunologically inert towards macrophages, and no inflammatory effect was detected *in vivo* [67]. Slight inflammatory effects were only detected with incorporated channel proteins [67]. Several drugs, proteins or nucleic acids can be encapsulated in polymersomes [36, 62]. To target polymersomes to a specific cell type, the polymersome surface has to be functionalized with sugars, aptamers, peptides and proteins, vitamins and antibodies [71]. Possible conjugation techniques are reviewed in Ref. [72].

1.2.3 Targeted Drug Delivery in Malaria

This section is based on a review by N. S. Santos-Magalhães and V. C. Furtado Mosqueira [73]. The main problems in antimalarial treatment are non-specific targeting of antimalarials to intracellular parasites and multiple drug resistance. The first problem is the reason why high doses of the drug are needed and this is one direct cause of the second problem. Nanotechnology provides new possibilities to overcome some of these drawbacks in malaria treatment. By encapsulating the antimalarial with a nanocarrier and subsequent functionalization of the nanocarriers with ligands specific for infected erythrocytes or hepatocytes, targeted drug delivery is possible. This leads to lower drug dose requirements for effective treatment, and other antimalarials that are more toxic than those commonly used could be examined, because the encapsulation shields the drug from the uninfected host cells. Therefore, adverse effects can be reduced, effective drugs with poor water solubility, low bioavailability, fast extracellular degradation and high toxicity can be tested, although they are not desirable if used without a carrier.

Three main strategies to target antimalarial loaded nanocarriers to infected cells are summarized in Fig. 4. A) and B) are both passive targeting strategies, whereas C) indicates active targeting with ligand-modified nanocarriers specific for infected cells.

Passive targeting makes use of the phagocytic activity of cells of the MPS. If nanocarriers are injected by the parenteral route, they are engulfed by MPS and the drug is released inside those cells. This strategy was studied in leishmaniasis therapy because the target host of *Leishmania* parasites are MPS cells. For example, primaquine, a schizontocidic drug which is very toxic, was encapsulated in nanocapsules and tested against leishmaniasis. It was shown that the toxicity can be reduced with this carrier system. In the case of malaria this strategy is not very promising because erythrocytes have

no phagocytic activity. Nevertheless, it is interesting that, with this approach, it is possible to slowly release a short half-life antimalarial drug from a depot (MPS) if loaded nanocarriers are taken up by MPS. For malaria treatment, the active targeting strategy (Fig. 4 C) seems to be more promising. But there are only a few attempts reported following this strategy. These attempts will be discussed in the following section.

Interestingly, it was shown that macromolecules such as dextran, protein A, IgG2a antibodies, anti-MSP1-42 antibodies, and even latex beads up to 80 nm in diameter could enter IEs and reach the parasite [74–76]. The reason why this is possible is still under debate. One explanation is the existence of a parasitophorous duct. This channel could exist because the site of merozoite invasion did not close after invasion [74]. Another possibility is that these particles can pass the 'leaky' erythrocytic membrane [76]. Nevertheless it can be hypothesized that nanocarriers up to 80 nm in diameter can enter IEs [73]. This would be a big advantage for targeted drug delivery to IEs.

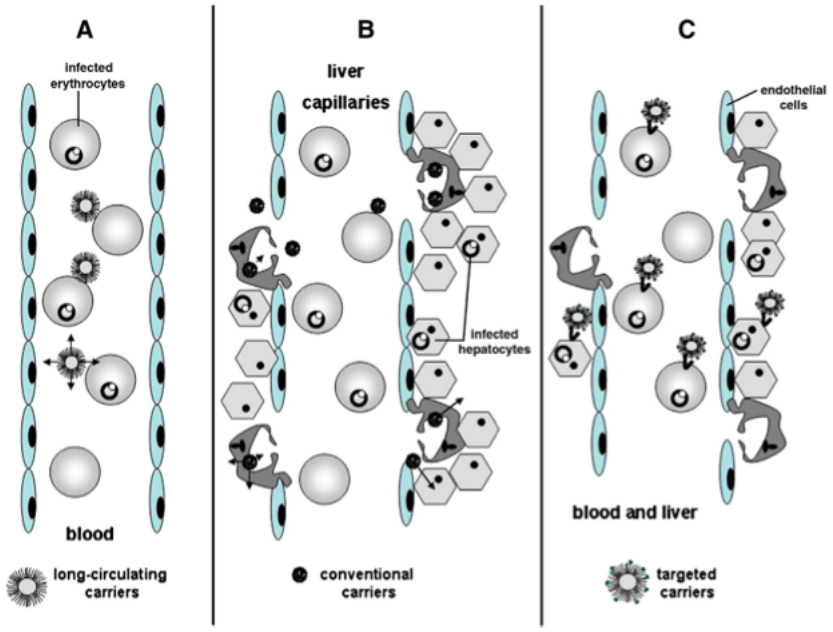

Figure 4: Summary of three conventional strategies for controlled drug delivery in malaria treatment. A) Long-circulating nanocarriers, B) conventional unmodified nanocarriers and C) ligand-modified nanocarrieres for targeted drug delivery [73].

One strategy uses the effective liver-targeting strategy of the malaria sporozoites [77]. The organ specificity can be related to two proteins on the sporozoite surface, circumsporozoite protein (CSP) and thrombospondin-related anonymous protein. It was shown that a conserved peptide (KLKQP) in CSP binds to highly sulfated heparan sulfate proteoglycans (HSPGs) found in the liver. The idea was to incorporate such peptides into liposomes to transport them specifically to the liver *in vivo*. In more detail, they used a peptide (acetyl-CKNEKKNKIERNNKLKQPP- amide) of the N-terminal region of the CSP of *P. berghei*, incorporated them into liposomes and injected them into mice where they were rapidly cleared form the blood stream. More than 80% of the liposome material was found in hepatocytes. As a major problem, intense serum-induced peptide-liposome aggregation was found. This can be overcome by using a certain mixture of lipids, lipid-polyethyleneglycol and lipid-

polyethyleneglycol-peptide.

Another approach is based on the functionalization of liposomes with antibodies specific for the target cell [78]. In this study, liposomes were filled with the commonly known antimalarial chloroquine and the liposome surface was modified with fragments of mouse antibodies MAb F_{10}. These antibody fragments are specific to *P. berghei*-infected mouse erythrocytes. With these liposomes it was shown that also chloroquine-resistent *P. berghei* infections in mice could be cured. A recent study used similar immunoliposomes with encapsulated chloroquine [79]. With this formulation, 8-fold less chloroquine concentration was needed for the same effect as free chloroquine. Interestingly, liposomes without specific antibodies for IEs were also targeted to IEs only, although with less efficacy.

The last example is focused on cerebral malaria, it is an active targeting strategy based on solid lipid nanoparticles (SLNs) [80]. One major problem with diseases of the brain is the lipophilic blood-brain barrier, which hinders water-soluble drugs from entering the brain. One solution is the use of suitable carrier systems. Quinine dihydrochloride is a drug to treat cerebral malaria but it is polar and needs a carrier system to reach the brain. Therefore, SLNs were loaded with quinine dihydrochloride and functionalised with transferrin. Transferrin receptors are expressed on the luminal membrane of brain endothelial cells and mediate the internalization of iron-saturated transferrin through receptor-mediated endocytosis. The uptake of quinine by the brain when using Transferrin-SLNs as carrier was 4 or 7 times higher compared with free drug or unfunctionalized SLNs, respectively.

For liposomes, it was proposed that they fuse with the membrane of IEs to release the drug to the parasite [79]. If nanocarriers (smaller than 80 nm) can reach the intraerythrocytic parasite, then, for example, pH-sensitve nanosystems can be used to release the drug efficiently, because the pH varies in the different compartments of an IE. Synthetic polymeric nanocarriers have not been highly exploited in the field of malaria. This should be done in the future [73].

2 Concept

Here, a new concept for the treatment of malaria is presented. The previous introductory sections reveal an interesting possibility to compete for merozoites. If it is possible to mimic the erythrocyte surface, mainly the important features for the initial contact between merozoites and erythrocytes, with artificial polymersomes, the merozoites will probably bind to these polymersomes as well.

Heparin-like molecules are thought to be the receptors on erythrocytes for first low-affinity contact with merozoites, via MSP1 proteins [15]. These molecules were proposed as possible candidates for a new drug formulation, although major problems remain unsolved at this time [15, 22]. It can be assumed that artificial polymersomes bearing heparin on their surfaces would bind and therefore compete for merozoites. If the interaction between these heparin-polymersome conjugates and merozoites is strong enough, the merozoites should not be able to invade new erythrocytes. One 200 nm object bound to a merozoite should be much more potent to prevent any new invasion of erythrocytes compared to some attached heparin molecules. The entry of heparin into IEs is not necessary for invasion inhibition, because immobilization of heparin on agarose beads also inhibited merozoite invasion [21]. With polymersomes of 200 nm in diameter one approaches the dimension of the active, invading site of merozoites. Merozoites are about 1.5 μm long.

On the other hand, nanocarriers are being examined in the context of targeted drug delivery to IEs [73]. Okoye and Bennett showed that human erythrocyte protein band 3 incorporated in liposome membranes can inhibit merozoites from invading new erythrocytes *in vitro* [81]. Therefore, it was decided to test whether heparin-polymersome conjugates could block erythrocyte invasion by merozoites.

The concept of invasion inhibition, by host cell mimicking polymersomes, is perhaps worth apply to other infectious diseases. In the search for whether a drug mimicking the host cell has already been used on any pathogen, it was found that a company called Nanoviricides Inc. is trying to mimic host cells of viruses with so-called nanoviricides^{TM} to fool the pathogen [82]. They functionalize nanomicelles with the receptors for viruses on host cells. These nanoviricides enwrap the virus, trap it, and the virus looses its coat proteins.

In the case of polymersomes, it was shown that bacterial channel-forming protein LamB can be reconstituted in ABA-triblock copolymer vesicles by fully preserving the function of LamB [83]. LamB is also the receptor for λ phage. Therefore, λ phages can bind to LamB in the vesicle membrane and inject their DNA into the artificial vesicles. In the previous section 1.2.1 it was mentioned that heparin may be a receptor for a number of different viruses. Therefore, a heparin-polymersome conjugate would probably bind to these viruses.

A more advanced strategy for the treatment of malaria is shown in the picture on the title page. The fact that it is possible to bring nanocarriers specifically to IEs [73] can be used to transport heparin-polymersome conjugates near the site of their action. A long spacer with an anti-IEs antibody on its end, for example, would be suitable to link the heparin-polymersome conjugates to IEs only. But maybe these conjugates are already targeted to IEs without the antibody, because it is known that a

specific variant of PfEMP1, appearing on the surface of IEs 24 h post-invasion, can bind heparin [32]. On the title page one IE is shown in the middle of the picture, immediately after the erythrocyte bursts. It sticks to the endothelium. The yellow merozoites enter the blood stream and are probably captured by the nearby heparin-polymersome conjugates. Dimensions of polymersomes and merozoites are presented in real proportion to erythrocytes.

In some way the point of view is changed with this strategy of merozoite invasion inhibition. For the development of a vaccine, a protein of the pathogen with low diversity and variability is sought-after. Diversity means differences between strains, whereas variability refers to changes in one parasite. If the focus is enlarged to the whole host-pathogen system, it would appear that the host is the stable part of this duo. The host is often highly diverse - human erythrocytes, for example [29] - but the host is less variable compared to the pathogen. Therefore, it seems to be a suitable strategy to mimic the host in order to fool the pathogen. It can be hypothesized that it is more difficult for the pathogen to gain resistance against such a drug. Resistance would mean that the pathogen no longer binds the functionalized polymersomes. But in this case the pathogen should no longer be able to bind to the host, unless it can bind to another feature on the host cell. Then, this new receptor on the host has to be identified and polymersomes could be changed accordingly to develop another functional drug.

Some other advantages of such a nanosystem compared to free sulfated glycosaminoglycans are the following. The half-life of these sugars in plasma is only about 1 hour [22, 51]. This could be one reason why *in vivo* experiments with monkeys and humans did not show any benefit upon heparin treatment [23, 24]. On the other hand, heparin-coated nanoparticles are long-circulating, up to 48 hours [43]. Furthermore, specific targeting to IEs would probably decrease the need for high dosages.

It should be mentioned that heparin in its natural form is not the molecule of choice for such an application, because of its anticoagulation properties. But similar molecules or modified heparin without or with lowered anticoagulation activity may be suitable [15, 33]. In this work heparin was chosen because of its availability and low cost. If the concept were to work with heparin, it can be hypothesized that similar molecules could be coupled to polymersomes as well. Whether they are active needs to be tested.

One remaining problem is the parenteral administration of such nanoparticle compounds. But oral administration is not impossible [40]. It was shown in rats that nanoparticles can cross the endothelial layer and enter the blood stream and were distribution to different tissues [84]. If these heparin-polymersome conjugates would have anti-rosetting- and anti-adhesion of IEs properties, parenteral administration would be no problem because this formulation would be an adjunctive treatment for severe malaria for already hospitalized patients.

Another interesting combination, which was not tested in this work, would be the encapsulation of heparin in nanospheres and targeting to IEs. Perhaps a formulation could be found to delivery this nanoparticles orally. Heparin would not be free in the blood stream; it would not exhibit its anticoagulation activity. Furthermore, heparin would be delivered into IEs only, where it could perhaps bind to the merozoites before their egress from the IE.

In this work we will see that two strategies to prepare heparin-polymersome conjugates, to test

their antimalarial activity were established. To prevent interference with the self-assembly of the polymersomes [65], heparin was tried to couple to the surface of already formed vesicles.

2.1 Heparin-Polymersome Conjugates by a Linker Chemistry

Many different methods for polymersome surface modification are known [72]. Egli *et. al.* introduced the linker system with hydrazinonicotinamide- and a formylbenzamide-counterpart functionalities for the surface modification of amine-terminated polymersomes [65]. The secondary amine groups on the polymersomes were modified to 4-formylbenzamide (4-FB) with succinimidyl-4-formylbenzoate (S-4FB) or poly(ethylene glycol)$_4$-pentafluorophenyl ester 4-formylbenzoate (PEG$_4$-PFB) and the desired ligands (eYFP and antibodies) were functionalized with succinimidyl-6-hydrazino-nicotinamide (S-HyNic). The reaction between those two linkers results in a stable, biocompatible and quantifiable bis-aryl hydrazone bond [65, 85, 86]. No catalyst is necessary and the reaction occurs in buffer solution.

This concept was applied in this work to couple heparin to polymersomes. Because heparin does not contain well accessible primary amino groups, such a group was inserted first. The method by V. D. Nadkarni *et. al.* was chosen to add a primary amino group to heparin and LMWH [87]. By this method 2,6 diaminopyridine (2,6-DAP) forms an imine with the reducing end of heparin only. This imine is stabilized by its reduction with sodium cyanoborohydride. The products are 2,6-diaminopyridinyl heparin (DAPH and DAPH-LWM) with a well accessible and free primary amino group. Then, the concept by Egli *et. al.* [65] was applied for the coupling of DAPH or DAPH-LMW to polymersomes by the described linker system.

2.2 One-Pot Synthesis of Heparin-Polymersome Conjugates

Another possibility to produce heparin-polymersome conjugates is a direct reductive amination. The reducing end of heparin can form an imminium ion with the secondary amine on the polymersome surface. This imminium ion is not stable in aqueous conditions. To get the stable tertiary amine the imminium ion has to be reduced with a suitable reducing agents.

This reaction was already performed with amine functionalized microspheres, heparin and sodium cyanoborohydride [88]. Sodium cyanoborohydride can reduce imines selectively over aldehydes or ketones, but a possible byproduct is highly toxic residual cyanide. Therefore, it was searched for a non-toxic variant of sodium cyanoborohydride, because for our purposes even the possibility of having highly toxic byproducts in the final product is not tolerable. Such a non-toxic, environmental friendly alternative is α-picoline-borane. It was shown that one-pot reductive amination of aldehydes with α-picoline-borane can be carried out successfully in aqueous solutions. It is still unknown why this reaction is possible in aqueous conditions. Because the formation of the imminium ion, which involves the elimination of a water molecule, would be expected to be highly disfavored in water. Nevertheless, Sato *et. al.* [89] have proven that this reaction works in water with similar yields compared to anhydrous conditions.

3 Materials and Methods

3.1 Chemicals

The following materials were used: heparin sodium salt from porcine intestinal mucosa (Sigma-Aldrich, 18 kDa), low molecular weight heparin sodium salt from porcine intestinal mucosa (LMWH, Sigma-Aldrich, 5 kDa), Oregon Green 488 succinimidyl ester (OG488-NHS, Invitrogen, *5-isomer*), sulforhodamine B (SRB, Invitrogen), mouse anti-heparin/heparan sulfate monoclonal antibody (Ab-Hep, Chemicon, Millipore, clone T320.11, 64kDa), toluidine blue (Fluka), protamine sulfate salt from salmon (Sigma-Aldrich, Grade X). The crosslinkers sulfo-succinimidyl-4-formylbenzoate (Sulfo-S-4FB), sulfo-succinimidyl-6-hydrazino-nicotinate acetone hydrazone (Sulfo-S-HyNic), and (polyethylene glycol)$_4$-penta-fluorophenyl ester formylbenzoate (PEG$_4$-PFB) were purchased from Solulink. The test reagents 2-hydrazino pyridine (2-HyPy) and 4-nitrobenzaldehyde (4-NB) were obtained from Sigma-Aldrich.

3.2 Buffers

The following buffers were used. After preparation the buffers were sterilised with 0.45 μm filters (Millipore). The composition of the buffers are not repeated in the following chapters.
- Modification buffer pH 7.4: 100 mM phosphate, 150 mM NaCl
- Modification buffer pH 8.3: 100 mM carbonate, 150 mM NaCl
- Conjugation buffer pH 6.0: 100 mM phosphate, 150 mM NaCl
- Conjugation buffer pH 5.0: 100 mM citrate, 150 mM NaCl
- Phosphate buffered saline (PBS) pH 7.4: 8.1 mM disodium hydrogen phosphate , 1.8 mM monopotassium phosphate, 2.7 mM KCl and 137 mM NaCl

3.3 Polymersome Formation

Diblock copolymer consisting of poly(dimethylsiloxane)-block-poly(2-methyloxazoline) (PDMS-*b*-PMOXA, AB) with hydroxyl (AB-OH) or piperazyl (AB-NH) functionalities at the hydrophilic terminus were synthesized and characterized by Dr. Stefan Egli (University of Basel). The synthesis plan and the characterization is presented elsewhere [65]. The PDMS block was purchased from ABCR (Germany), whereas the hydrophilic oxazoline blockpolymerisation and the functional terminations were subsequently carried out. The chemical composition of the diblock copolymers is presented in the following figure 5.

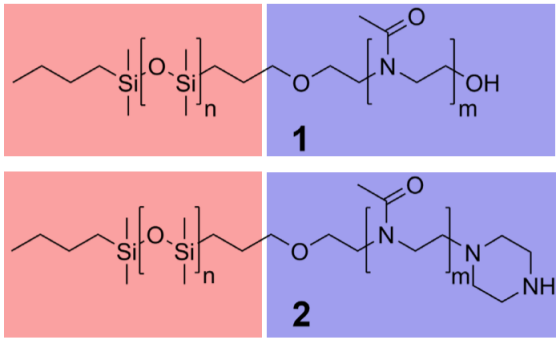

Figure 5: PDMS-*b*-PMOXA diblock copolymer structures, with either hydroxyl (**1**, AB-OH) or piperazyl functionality (**2**, AB-NH) at the hydrophilic end [65]. The hydrophobic part is highlighted in red, the hydrophilic block in blue.

The molar masses for AB-OH and AB-NH were 6139 g/mol and 6185 g/mol, respectively. The block lengths were calculated from ^{1}H-NMR. AB-OH was shown to be composed of 65 siloxane units and 13 2-methyloxazoline units, and the AB-NH of 68 siloxane units and 11 2-methyloxazoline units.

Vesicles were formed using the film hydration method. First, mixtures of the desired ratio of AB-OH and AB-NH were dissolved in ethanol (6 mg/ml) and put in a round bottom flask. Subsequently, the solvent was removed in a rotary vacuum evaporator (100 mbar, 40°C, 120 RPM). A smooth polymer film forms inside the flask. To evaporate the solvent completely, the film was further dried under vacuum for approximately two hours. Afterwards, the film was hydrated with a defined volume of modification buffer pH 8.3 to obtain polymersome solutions of 3 mg/ml polymer concentration. Polymersomes were formed at room temperature under stirring for typically two days. Subsequently, the polymersome solutions were extruded using a LIPEX^{TM} extruder (Northern Lipids Inc., Canada). The polymersomes were pushed four times through a nucleopore track-etch membrane with an average pore diameter of 0.4 µm (Whatman, GE Healthcare, UK) and then 20 times through a nucleopore track-etch membrane with an average pore diameter of 0.2 µm to get a homogenous solution of polymersomes with 200 nm in diameter. Samples containing unmodified polymersomes consisting of 5% AB-NH and 95% AB-OH (3 mg/ml) are called V-NH in the following.

For fluorescence correlation spectroscopy (FCS) measurements, a polymer film was hydrated with a 0.6 mM sulforhodamine B (SRB) solution in PBS. After extrusion through the desired nucleopore track-etch membrane, extensive dialysis against 100 mM NaCl and in a last step against PBS were performed in order to get rid of non-encapsulated SRB.

3.4 Fluorescence Labeling

Fluorescence labeling was performed for the detection of heparin by fluorescence correlation spectroscopy (FCS). Standard succinimidyl-ester activated dyes were used to couple the desired dye to primary amino groups on biomolecules.

3.4.1 Heparin Labeling

Amino groups of DAPH and heparin were labeled with Oregon Green 488 succinimidyl ester (OG488-NHS). 0.5 mg of each sugar was dissolved in 50 µl modification buffer pH 7.4 (10 mg/ml, 28 nmole) and an 3.5 excess of OG488-NHS in DMSO (5 µl, 100 nmole) was added. After four hours incubation under shaking at room temperature the products were purified from free OG488 by fast protein liquid chromatography (FPLC Äkta, Amersham Biosciences) with a Sephadex^{TM} G25 column and PBS as eluent. The products were analyzed using UV/Vis absorbance and FCS measurements.

3.4.2 Protein Labeling

Anti-heparin antibodies (AbHep) and protamine were fluorescently labeled with OG488-NHS. 5.1 mg protamine sulfate was dissolved in 500 µl modification buffer pH 8.3 (10.2 mg/ml, 1 µmole). 0.5 mg OG488-NHS was dissolved in 50 µl DMSO (1 µmole) and subsequently added to the protamine solution. The mixture was incubated under shaking at room temperature for four hours. The product was purified from free OG488 by fast protein liquid chromatography (FPLC Äkta, Amersham Biosciences) with a Sephadex^{TM} G25 column and PBS as eluent.

In case of AbHep the buffer of 100 µl AbHep (1 mg/ml, 1.6 nmole) in 20 mM sodium phosphate, 250 mM NaCl, pH 7.6, with 0.1% (w/v) sodium azide was exchanged to modification buffer pH 8.3 using centrifugal filters (Amicon Ultra 500 µl, Millipore, Ireland, MWCO = 10kDa). 80 µl AbHep (1.25 mg/ml, 1.6 nmole) was recovered and a 12 fold excess of OG488 over antibody concentration in DMSO (1 µl, 19.6 nmole) was added. After 3.5 hours incubation under shaking at room temperature, the mixture was filled up to 500 µl and the product was purified from free OG488 by fast protein liquid chromatography (FPLC Äkta, Amersham Biosciences) with a Sephadex^{TM} G25 column and PBS as eluent. All products were analyzed using UV/Vis absorbance and FCS measurements.

3.5 Heparin Detection

3.5.1 Toluidine Blue Microassay

Toluidine blue microassay was performed according to MacIntosh [90] and Smith *et. al.* [91] with slight modifications. Essentially, the assay was scaled down in order to use smaller amounts of sample in the range of some micro liters. First, 2.5 mg toluidine blue was dissolved in 50 ml 10 mM HCl containing 0.2% (w/v) NaCl. This leads to a 0.005% (w/v) stock solution of toluidine blue. Secondly, standard heparin solutions were prepared. Either 180 µg/ml LMWH (25.2 USP/ml) or 140 µg/ml heparin (25.2 USP/ml) in 0.2% (w/v) NaCl were used to get standard curves for the toluidine blue microassay. 250 µl toluidine blue were put in 1.5 ml Eppendorf tubes. 5 to 40 µl of the standard heparin solutions or the heparin-polymersome samples were added and each tube was filled up to 500 µl with 0.2% (w/v) NaCl. After vigorous mixing for 30 seconds 500 µl n-hexane was added to each tube to bring the insoluble heparin-dye complexes to the water-hexane interphase. After another 30 seconds vortexing and incubation for some minutes 30 µl of the water phase of each sample was

pipetted into 120 µl ethanol. UV/Vis absorbance measurements of these ethanol-sample mixtures at 631 nm showed typical dye depletion as reported in [91].

Naked eye detection was possible in about the same range as for the whole procedure described above. Here 5 µl toluidine blue and 5 µl sample were mixed. By eye the presence of heparin was visible as the color changes with increasing heparin concentration from light blue to dark blue and purple in the end.

3.5.2 Fluorescent Proteins

The concentration of fluorescent protamine or antibody after FPLC could not be determined, because protamine does not absorb at 280 nm (no tryptophan) and the extinction coefficient of the antibody is not known. But the mixture were prepared to obtain optimal conditions for FCS measurements, which is the nano molar region. In the following chapters these detection methods are called protamine test and antibody test.

If the samples where measured after mixing without further purification 4 µl sample was mixed with 1 µl ProtOG488 (1/100 of stock) in PBS or AbHepOG488 (1/10 of stock) in PBS, respectively. In case of the antibody, the mixtures were incubated at room temperature for at least half an hour before measured with FCS. If the mixtures were purified before FCS measurements more sample volume was necessary that size exclusion chromatography (SEC) was possible. Typically, 50 µl sample was mixed with 2 µl ProtOG488-stock or 10 µl AbHepOG488-stock. ProtOG488 mixtures were incubated for 1.5 hours, and AbHepOG488 mixtures for three hours. After subsequent SEC on Sepharose 2B in PBS the polymersome fractions were concentrated to about 40 µl using centrifugal filters (Amicon Ultra 500 µl, Millipore, Ireland, MWCO = 100 kDa) before FCS measurements. As a negative control 50 µl V-NH in PBS was mixed with free OG488, incubated at room temperature for three hours, purified by SEC on Sepharose 2B in PBS, and concentrated with centrifugal filters (MWCO = 100 kDa) before FCS measurement.

3.6 One-Pot Synthesis of Heparin-Polymersome Conjugates

One-pot reductive amination was carried out according to Duo *et. al.* [88] but with the non-toxic reducing agent α-picoline-borane instead of sodium cyanoborohydride. About 1.5 mg heparin was dissolved in 1 ml V-NH (3 mg/ml polymer, 5% AB-NH, modification buffer pH 8.3). A tip of a spatula α-picoline-borane was added to the solution. This mixture was incubated under shaking at room temperature for at least 4 days. To purify the heparin-polymersome conjugates from free heparin SEC on a Sepharose 2B column in PBS was performed.

3.7 Synthesis of 2,6-Diaminopyridinyl Heparin

2,6-Diaminopyridinyl heparin (DAPH) was synthesized and purified according to the protocol by V. D. Nadkarni *et. al.* [87]. First it was carried out with LMWH (mean MW = 5kDa) and secondly

with full length heparin (mean MW = 18kDa). The procedure will be described with LMWH and the conditions for unfractioned heparin are listed at the end of this section.

First 200 mg LMWH (40 µmole) was dissolved in 4ml formamide in a two-neck round bottom flask with a stirring bar under argon at 50°C. After about two hours the sugar was completely dissolved. Then, a 100 fold excess of 2,6-diaminopyridine (2,6-DAP) was added (440 mg, 4 mmole) and incubated for six hours under the mentioned conditions and shaded from light. Subsequently, a 20 molar excess of the reducing agent sodium cyanoborohydride (50.2 mg, 0.8 mmole) was added and the mixture was incubated at 50°C for 24 hours. The reaction was quenched with 10 ml double distilled water (ddH_2O) and the mixture was dialyzed against two liters ddH_2O (Spectra/Por®Biotech, Cellulose Ester, Dialysis Membranes, MWCO = 500-1000 Da, Spectrum Laboratories, USA) for about 60 hours and then it was lyophilized. For additional purification of the sample, methanol precipitation was carried out. The lyophilized sample was redissolved in 3 ml 16% (w/v) NaCl solution and 12 ml cold methanol was added dropwise to the sample. And the sample was allowed to precipitate overnight at 4°C. After centrifugation for 10 min at 3000 RCF the supernatant was discarded and the precipitation was repeated for at least two times. The last pellet was dissolved in ddH_2O, dialyzed extensively against ddH_2O (MWCO = 500-1000 Da) and lyophilized.

In a first trial strong anion exchange chromatography (SAX) was also performed to further purify the sample. But for some unknown reasons the sample recovery was only about 2% after SAX and it was found that the sample was already clean enough for our purposes before SAX. For these reasons the purification was stopped after methanol precipitation and the second dialysis step.

The amounts of chemicals used for the synthesis of DAPH were the following: 100 mg heparin (5 µmole), 1ml formamide, 100 mg 2,6-DAP (917µmole), and 9.5 mg sodium cyanoborohydride (0.15 mmole). All other conditions, reaction times, and purification steps were the same as for LMWH.

3.8 Modification of DAPH

DAPH and DAPH-LMW were dissolved in modification buffer pH 7.4 to reach concentrations of about 27 mg/ml or 50 mg/ml, respectively. Then, aliquots of 50 mM sulfo-succinimidyl-6-hydrazinonicotinate acetone hydrazone (Sulfo-S-HyNic) in DMSO were added to the solutions. A 25 fold excess of Sulfo-S-HyNic over DAPH was used and for DAPH-LMW a three fold excess. Typical reaction mixtures for the modification of DAPH with Sulfo-S-HyNic were the following: 0.8 mg DAPH, 30 µl modification buffer pH 7.4, 20 µl of 50 mM Sulfo-S-HyNic in DMSO. These mixtures were incubated under shaking at room temperature for about three hours. Afterwards, the samples were filled up to 500 µl with modification buffer pH 7.4 and DAPH-HyNic was purified from free HyNic with several diafiltration steps using centrifugal filters (Amicon Ultra 500 µl, Millipore, Ireland, MWCO 10 kDa or 3 kDa). After 10 times 5 min (MWCO = 10 kDa) or 10 times 10 min (MWCO = 3 kDa) diafiltration with modification buffer pH 7.4 at 13,400 RPM about 80 µl of purified samples were recovered.

To check the coupling reaction 5 µl of the purified sample, 5 µl of the rest from the last diafiltration

step and 5 µl buffer were mixed with 100 µl 0.5 mM 4-nitrobenzaldehyde (4-NB) in conjugation buffer pH 5.0. These mixtures were incubated at 37°C for one hour. Subsequent UV/Vis absorbance measurements were recorded in the range from 220 nm to 450 nm. Schematic presentations of the modification and conjugation reactions were drawn using ChemDraw and NeoOffice.

3.9 Modification of Polymersomes

Typically, a 50 fold excess of sulfo-succinimidyl-4-formylbenzoate (Sulfo-S-4FB) or poly(ethylene glycol)$_4$-pentafluorophenyl ester formylbenzoate (PEG$_4$-PFB) (40 µl, 50mM in DMSO) over AB-NH concentration was put in 360 µl modification buffer pH 8.3 and this mixture was added immediately to 1.6 ml polymersome solution (3 mg/ml, 5% AB-NH, conjugation buffer pH 8.3). After three hours incubation under shaking at room temperature the modified polymersomes (V-4FB, V-PEG4FB) were purified from the excess of linkers by extensive dialysis against 100 mM NaCl (MWCO = 300 kDa). In a last step, the dialysis bath was changed to conjugation buffer pH 6.0.

To test the two different available linkers for polymersome modification a single polymersome solution (3.2 ml, 3 mg/ml, 5% AB-NH) was split into two equal portions. To one half of the polymersome solution a 50 fold excess of Sulfo-S-4FB (40 µl, 50 mM in DMSO) over AB-NH, to the other half the same excess of PEG$_4$-PFB (40 µl, 50 mM in DMSO) was added. After three hours incubation under shaking at room temperature the solutions were dialyzed against 100 mM NaCl, in a last step against conjugation buffer pH 6.0. Subsequently, to 900 µl of each sample a 14 fold excess of 2-hydrazino pyridine (2-HyPy) in conjugation buffer pH 6.0 (100 µl, 275 mM) over AB-NH was added to test bis-aryl hydrazone bond formation with the 4-FB moieties on the polymersomes. After 4h incubation under shaking at 37°C the samples were dialyzed again against 100 mM NaCl overnight and then against ddH_2O. Afterwards, the samples were lyophilized and redissolved in 150 µl ethanol for UV/Vis absorbance measurements.

3.10 Conjugation of Heparin to Polymersomes

Polymersome-heparin conjugates (V-DAPH) were produced by mixing 1 ml of 4FB modified polymersomes (V-4FB or V-PEG4FB) in conjugation buffer pH 6.0 or pH 5.0 with 80 µl DAPH-HyNic (0.9 mg/ml) in conjugation buffer pH 6.0 or modification buffer pH 7.4. These mixtures were incubated under shaking at room temperature for at least 16 hours. For the purification of excess DAPH from V-DAPH several methods were used. The tested methods were extensive dialysis against 100 mM NaCl and in a last step against PBS (MWCO = 300 kDa), FPLC with a Superdex^{TM} 200 10/300 GL column in PBS, or SEC on Sepharose 2B in PBS.

3.11 Preparation of Polymersome-eYFP conjugates

Polymersome-eYFP conjugates were prepared according to Ref. [65] (Supplementary Information). Primary amino groups of eYFP were modified with S-HyNic and subsequently coupled to

V-PEG4FB.

A 12 fold excess of S-HyNic in DMSO (10 µl, 100 mM, 1 µmole) over eYFP concentration was dissolved in 110 µl conjugation buffer pH 7.4 and this mixture was added to an eYFP solution in conjugation buffer pH 7.4 (80 µl, 963 µM, 77 nmole). This leads to a reaction concentration of 12 mg/ml for eYFP. After incubation under shaking at room temperature for 3 hours residual HyNic was separated from eYFP-HyNic conjugates by eight diafiltration steps with centrifugal filters (MWCO = 10 kDa) with conjugation buffer pH 6.0. A total volume of 55 µl eYFP-HyNic solution was recovered. 5 µl were used to test the linker availability on eYFP, 25 µl were added to 1 ml V-PEG4FB in conjugation buffer pH 6.0, and the remaining 25 µl to 1 ml V-NH in conjugation buffer pH 6.0 as a negative control. After incubation under shaking at room temperature for three days polymersome-eYFP conjugates were purified from excess eYFP-HyNic by SEC on Sepharose 2B in PBS and the samples were concentrated with centrifugal filters (MWCO = 100 kDa) before FCS measurements.

3.12 Fluorescence Correlation Spectroscopy

Fluorescence correlation spectroscopy (FCS) measurements were performed on a commercial Confocor2 (Carl Zeiss, Jena, Germany). An Ar^+ laser at a wavelength of 488 nm was used as the excitation source. The excitation power was set to 60% of 30 mW, with an excitation transmission between 2% and 10%. The light passed a dichroic beam splitter (DBS HFT 488) and was focused onto the sample through a C-Apochromat 40x water immersion objective with a numeric aperture of 1.2. The fluorescence signal was collected through the same objective, and passed through the DBS again. To detect the desired emission frequencies only and from the desired confocal volume, a long pass (LP 505) filter followed by a pinhole were used. The pinhole diameter was set to 70 µm. Finally, the fluorescence intensity was recorded with an avalanche photodiode (APD). All FCS measurements were performed at room temperature (24°C).

Typically, a drop of 5 µl sample was used for one measurement. Before one measurement series the pinhole was always adjusted using free dye to record maximum intensity in all measurements. Normally, measurement series of 10 times 5 s for fast diffusing species (labeled proteins) and 10 times 10 s for slowly diffusing species (polymersomes) were recorded in triplicate. In data tables the mean value over these 30 measurements and the corresponding standard deviation are presented. FCS curves were processed using the ConfoCor3 software. All graphs were drawn using R Statistics. For FCS curve analysis the structural parameter R, which describes the confocal volume, was set to 5. Furthermore, a triplet fraction was always included and fixed to 3 µs if the initial fit gave a value higher than 10 µs. All FCS curves were normalized in order to compare the shifts in the diffusion times.

The following equations were needed to get the experimental autocorrelation curve (Eq. 1), the fit for the experimental autocorrelation curve (Eq. 2, 3), the diffusion coefficient (Eq. 5), and the hydrodynamic radius of the diffusing species (Eq. 6). To autocorrelate the intensity signal equation 1 was used. I(t) and I(t+τ) represent the fluorescence intensity at a given time t and after a certain delay

time τ, respectively [92].

$$G(\tau) = 1 + \frac{< \delta I(t) \delta I(t+\tau) >}{< I(t) >^2} \tag{1}$$

The experimental autocorrelation curves were fitted with a 3D diffusion fitting model for Brownian motion in a Gaussian volume element (Eq. 3). These autocorrelation function contains three different parts. In the following equations only one diffusing species is assumed to simplify the terms.

$$G(\tau)_{fit} = G_{inf} X_{Triplet} \frac{1}{N} G(\tau) \tag{2}$$

G_{inf} the value at infinite τ, $X_{Triplet}$ a term which corrects for intersystem crossing (molecules in triplet state) and $G(\tau)$ the 3D diffusion term.

$$G(\tau)_{fit} = 1 + (1 + \frac{T}{1-T} e^{-\tau/\tau_{trip}}) \frac{1}{N} \left[\frac{1}{1+\frac{\tau}{\tau_D}} \frac{1}{\sqrt{1+R^2 \frac{\tau}{\tau_D}}} \right] \tag{3}$$

T is the fraction of fluorophores in the triplet state, τ_{trip} is the corresponding triplet time, N the number of particles, and R the structural parameter. The Einstein-Stokes equation (Eq. 4) describes the relation between the diffusion constant D of a diffusing spherical particle with its hydrodynamic radius R_H.

$$D = \frac{k_B T}{6\pi\eta R_H} \tag{4}$$

k_B is the Boltzmann's constant, T the absolute temperature, and η_{medium} the viscosity of the surrounding medium. If the x-y dimension ω_{xy} of the confocal volume is known the diffusion constant D can be calculated with the measured diffusion time τ_D and the following equation 5.

$$\tau_D = \frac{\omega_{xy}^2}{4D} \tag{5}$$

By combining the two equations 4 and 5 the hydrodynamic radius R_H can be determined via the diffusion time τ_D got from the FCS fit (Eq. 3).

$$R_H = \frac{4 k_B T \tau_D}{6\pi\eta\omega_{xy}^2} \tag{6}$$

3.13 Chromatography

Fast protein liquid chromatography (FPLC) and strong-anion exchange chromatography (SAX) were performed on an Äkta system (Amersham Biosciences). The used columns were Superdex^{TM} 200 10/300 GL, Sephadex^{TM} G25, or in case of SAX a HiPrep 16/10 Q FF column. Size exclusion chromatography (SEC) was performed on a Sepharose 2B column.

3.14 UV/Vis Absorbance Measurements

UV/Vis absorbance measurements were performed on a SpectraMax Plus 384 (Molecular Devices, Sunnyvale, California) using 0.1 ml cuvettes. Intact polymersome solution were measured on a Specord 210 plus (Analytik Jena, Jena, Germany). To get the extinction coefficients for 2,6-DAP at 240 nm and 333 nm, calibration curves were determined using 100 μM, 75 μM , 50 μM , 25 μM , and 12.5 μM solutions of 2,6-DAP in conjugation buffer pH 5.0.

3.15 NMR

^{1}H-NMR spectra were recorded on a Bruker DPX-400 NMR spectrometer in D_2O at room temperature. As a reference the solvent peak was set to a chemical shift of 4.79 ppm. The spectrometer was operated at 400 MHz and 128 NMR cycles were recorded for each sample.

3.16 TEM

For transmission electron microscopy (TEM) polymersome solutions were negatively stained with 2% uranyl acetate solution and deposited on a carbon-coated copper grid. The samples were recorded with a transmission electron microscope (Philips Morgagni 268D) at an acceleration voltage of 80 kV.

3.17 Biological Experiments

Parasite cultures were carried out as described elsewhere [93]. Polymersome solutions were sterilized by filtration through 0.45 μm pore filters. The 3D7 isolate of *P. falciparum* was used. For the vesicle uptake experiment polymersome solutions with 3 mg/ml polymer (V-SRB, 100% AB-OH) in PBS and 0.6 mM SRB incorporated were needed. Parasites were cultured in the presence of V-SRB over at least one whole cycle of parasite replication. For the growth inhibition assay (GIA) parasites were cultured in the presence of heparin or V-DAPH over at least one whole cycle of parasite replication. The typical start parasitemia was 0.2 % in 10 ml culture plates with 3% hematocrit. After three days incubation, thin blood smears were made and Giemsa staining was carried out to visualize the parasites. The blood smears were examined by bright field and fluorescence microscopy.

4 Results and Discussion

4.1 Polymersome Formation

Polymersomes formed by using the film rehydration technique were analyzed by FCS and TEM. Normally, polymersomes with 200 nm diameter were produced. To get smaller diameters e.g. nucleopore track-etch membrane with an average pore diameter of 0.08 μm (Whatman, GE Healthcare, UK) were used for extrusion. The lower limit in diameter for hollow polymersomes probably lies around 50 nm, with a membrane thickness of about 15 nm for this polymer [65].

The FCS measurements of the polymersome solutions after dialysis are shown below (Fig. 6) and the corresponding data from the fits are listed in a table (Tab. 1). The data in the table are mean values and standard deviations for 3 x 10 x 10 seconds measurement series. To calculate the hydrodynamic radius (R_H) a beam waist of (200±7) nm for the argon laser at 514 nm excitation wavelength was used [94].

	SRB	V-SRB-200nm	V-SRB-80nm
Diffusion time τ_D [μs]	25.5±0.6	5694±658	2688±61
R_H [nm]	0.53±0.01	118±14	56±1

Table 1: Diffusion time and R_H from FCS measurements of SRB encapsulated in polymersomes with 200 nm and 80 nm diameter, respectively .

The calculated hydrodynamic radii of V-SRB-200 nm and V-SRB-80 nm are somewhat bigger than expected. One reason could be that the actual beam waist was larger than calculated. Or, as can be seen in the TEM pictures of 200 nm polymersomes (Fig. 7), the samples did not consist of polymersomes with uniform diameters. Some have diameters up to 500 nm and some are much smaller than 200 nm (e.g. micelles). Therefore, the FCS data can be taken as mean values but the effective error is bigger than calculated. Nevertheless, most importantly there is a measurable difference of about a factor of two between 200 nm and 80 nm diameter polymersome samples. This is also directly observable in the shifts of the FCS curves (Fig. 6). As reported previously, this polymer forms mostly vesicular structures [65]. From the TEM pictures it is known that some micelles and worm-like micelles were also obtained.

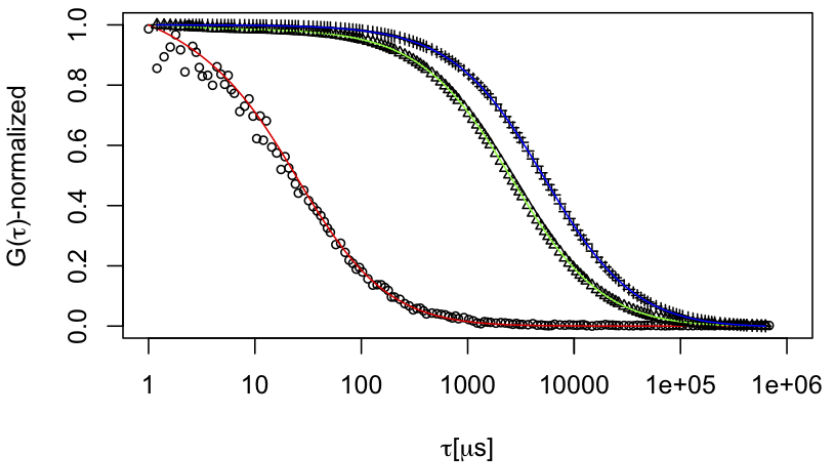

Figure 6: Normalized autocorrelation curves from FCS measurements with free SRB in PBS (dots, red fit), V-SRB-80nm (triangles, green fit), and V-SRB-200nm (crosses, blue fit).

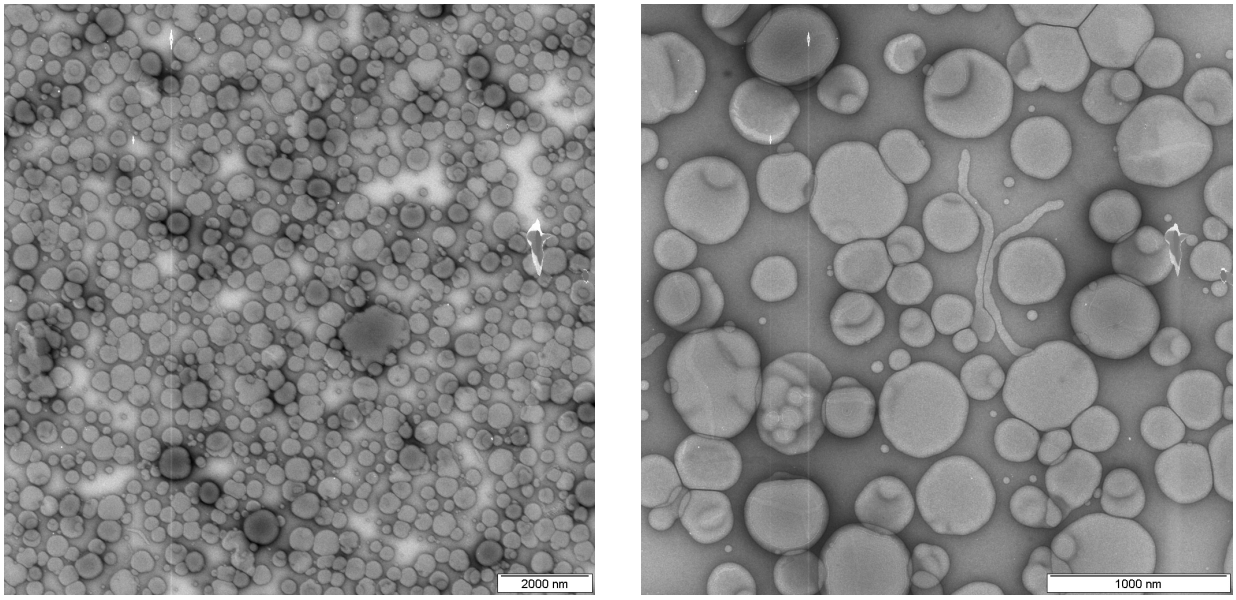

Figure 7: TEM pictures of polymersomes extruded through 0.2 μm. Left, an overview in which primarily vesicular structures can be observed. Right, detailed picture with micelles (small dots), vesicles (big spheres) and two worm-like micelles (middle).

4.2 Fluorescence Labeling

Fluorescence labeling of heparin and protamine was first carried out with Atto647-NHS (Fluka). But some difficulties arose. Yields of fluorescently labeled biomolecules were low and purification with centrifugal filters or dialysis did not work properly. Furthermore, nonspecific binding to polymersomes was observed, which led to polymersome aggregation. Therefore, it was decided to change

to another reactive dye, OG488-NHS (Invitrogen). Also, FPLC was used for purification instead of centrifugal filters or dialysis.

The results for OG488-labeled protamine and AbHep after FPLC purification are listed below (Tab. 2, Fig. 8). The data for OG488-labeled heparin are in section 4.5 (Fig. 14). In the case of protamine, the N-terminus of the protein was labeled, because this protein has no lysine residues. This led to a maximum of one dye per protamine molecule, ensuring that it was not possible to overmodify the protamine with too many fluorescent molecules. The positively charged arginine residues on protamine must be accessible for the electrostatic interaction to occur between heparin and protamine. On the other hand, antibodies contain several lysine groups on their surfaces, which leads to fluorescence labeling at different positions. These attached fluorescent molecules can interfere with the specific binding ability of the antibody. A way to circumvent this problem is the use of a labeled secondary antibody which recognizes mouse antibodies, instead of labeling the primary antibody. However, for FCS measurements, such a system is not favorable because too many different components are present, and drawing conclusions from these data is very complex. Therefore, it was decided to label the primary antibody, although this was not fully satisfactory.

	OG488	ProtOG488	AbHepOG488
Diffusion time τ_D 1st Fraction [µs]	-	26.3 fixed	23.5 fixed
1st Fraction [%]	-	15	12
Diffusion time τ_D 2nd Fraction [µs]	26±2	84±6	221±16
2nd Fraction [%]	100	85	88
R_H 2nd Fraction [nm]	0.56±0.04	1.8±0.1	4.7±0.3

Table 2: Diffusion time τ_D and R_H from FCS measurements of free OG488, ProtOG488, and AbHepOG488 in PBS.

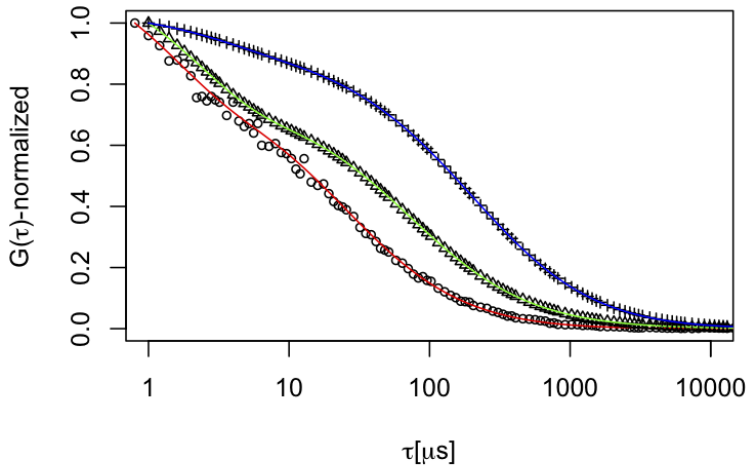

Figure 8: Normalized autocorrelation curves from FCS measurements with free OG488 in PBS (dots, red fit), ProtOG488 (triangles, green fit), and AbHepOG488 (crosses, blue fit).

The FCS data show clearly that protamine and antibodies were successfully labeled with OG488. The diffusion time increases with higher molecular weight in the expected order: OG488 (0.51 kDa), protamine (5.1 kDa), and AbHep (64 kDa).

But even though the samples were purified by FPLC, there was always some residual OG488 measurable in both samples. This could mean that OG488 also binds non-covalently to the proteins and elutes in the protein fraction. Afterwards, these non-covalently bound OG488 molecules can dissociate from the proteins and give rise to the fractions of 15% and 12% for free OG488 in ProtOG488 or AbHepOG488 samples, respectively (Tab. 2). These data were measured directly after the coupling reaction and purification. During the next two months the fractions of free OG488 increased to about 50% in the same samples. In conclusion, these conjugates were not very stable over time but, keeping this in mind, FCS measurements are still possible with these proteins. In the future, purification of labeled proteins from residual dye should be tried with reverse phase high-performance liquid chromatography (RP-HPLC). With this method the separation of labeled proteins from free dye would improve and it may even be possible to separate unlabelled- from labeled proteins.

4.3 Heparin Detection

The detection of heparin was one of the most critical steps in this whole project. With well-established colorimetric methods, such as the toluidine blue assay (Ref. [91]), the detection limit was at the border of usefulness. On the other hand, the use of fluorescent proteins that bind specifically to heparin, followed by FCS measurements is a much more sensitive method. But also with this method several difficulties were observed, as described later in this work. We will see that none of the used methods was really satisfactory. There was no more time to test new advanced detection methods. In particular because it would first include the synthesis of a probe molecule. Some ways of detecting heparin are listed in the following reference [95].

Another method of detection is based on self-quenching of fluorescein-labeled protamine (FITC-protamine) as it accumulates on heparin chains [96]. This was tested in this case as well, but the detection limit was not lower than for the toluidine blue assay. Therefore, the toluidine blue microassay was used, along with FCS measurements of fluorescent proteins that should have been specifically bound to heparin. The interaction of ProtOG488 and heparin was investigated (Sect. 4.3.2), but it was not possible for the AbHepOG488. AbHepOG488 and AbHepOG488-heparin conjugates cannot be distinguished by FCS. Another possibility would be the detection of heparin by its biological anticoagulation properties. But there was no more time to perform this anticoagulation assay. In particular, it is not known whether heparin that is immobilized on polymersomes by this method still bears this property. If undetectable, it would again not be possible to verify whether the coupling of heparin to polymersomes took place.

4.3.1 Toluidine Blue Microassay

The toluidine blue assay was used as described by MacIntosh [90] and Smith *et. al.* [91]. The metachromatic dye, toluidine blue, binds to polyanionic substrates. Upon binding there is a shift in the absorption spectrum. When the toluidine blue solution was mixed with an equal volume of PBS containing at least 20 µg/ml LMWH or 16 µg/ml heparin, the color change was visible with the naked eye. The solution changed from light blue to dark blue. With higher heparin concentrations, the mixture became purple. This naked-eye detection was only useful to determine whether heparin was present at a concentration in a solution higher than the detection limit. The procedure described in section 3.5.1 had to be performed in order to acquire the absolute concentration of heparin.

Standard curves for the micro toluidine blue assay are presented in the following figure 9. For LMWH the linear fit (left, $y = -0.060x + 0.731$, R^2=0.955) is shown in red, for heparin in blue (right, $y = -0.0714x + 0.728$, R^2=0.941). Because of the metachromatic band overlap, the detection of heparin is not possible directly. After mixing the toluidine blue solution with standard heparin concentrations or with heparin-polymersome conjugates, the insoluble heparin-dye complexes had to be removed from the solution before measuring the absorbance at 631 nm. When more heparin was present, more heparin-dye complexes formed, and therefore less dye was left in the solution after removing the heparin-dye complexes.

The standard curves are linear for dye depletion of 10 - 50% [91]. The heparin-dye complexes were removed by adding n-hexane to the mixture. The complexes precipitated at the water-hexane interface and, for subsequent absorbance measurements, the water phase was pipetted out. Smith *et. al.* [91] showed that removal of heparin-dye complexes is possible by centrifugation if heparin is immobilized on Sepharose 4B. In the case of heparin-polymersome conjugates, n-hexane, filtration (0.2 µm pore diameter) or centrifugal filters (MWCO = 3 kDa) were tested. With the centrifugal filters no reproducible results were obtained, with normal filters this was possible. But in the end the original method with n-hexane was used. Hexane dissolved the polymersomes and the polymer also accumulated at the water-hexane interface. Most probably the hydrophilic head of the AB-polymer was in the water phase, whereas the hydrophobic part pointed into the organic phase.

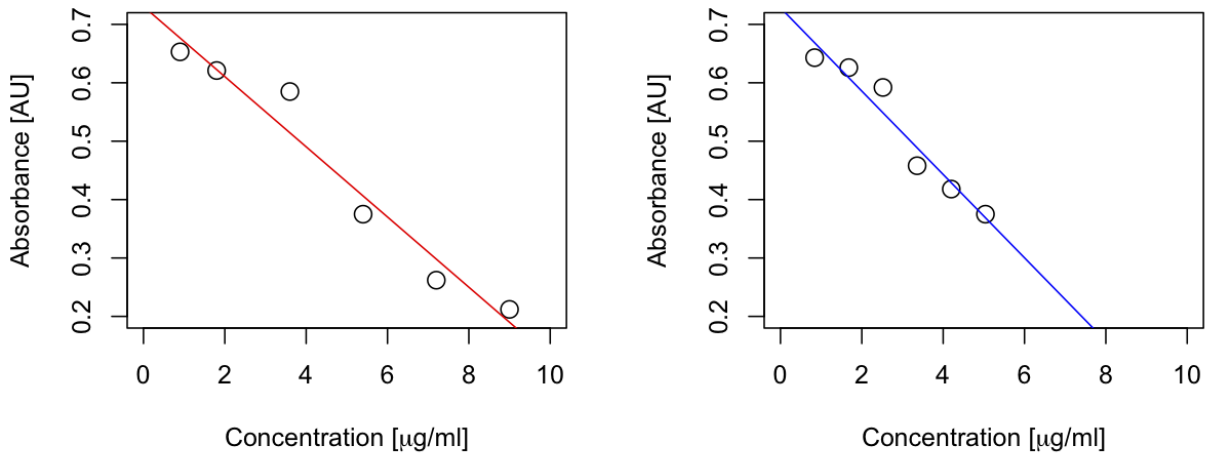

Figure 9: Standard curves for toluidine blue microassay. With increasing heparin concentration the absorbance measured at 631 nm decreases. The left figure (red fit) represents the standard curve for LMWH and the right figure (blue fit) the standard curve for full-length heparin.

4.3.2 Interaction of Heparin and ProtamineOG488

The use of fluorescent protamine for the detection of heparin-polymersome conjugates using FCS was already described elsewhere [47]. Protamines are small, highly positively charged peptides which bind specifically to heparin with high affinity. Very strong ionic interactions between the negatively charged sulfo- and carboxyl groups of heparin and the positively charged arginine residues on protamine are formed.

To check this interaction, mixtures of ProtOG488 in PBS containing 144 µg/ml LMWH or 112 µg/ml heparin were analyzed by FCS measurements (Fig. 10). The typical diffusion times for free OG488, ProtOG488, and heparin-OG488 are listed elsewhere in this work: (26±2) µs, (84±6) µs, and (166±26) µs, respectively (Tab. 2, 4). As shown below, heparin and ProtOG488 formed aggregates, as expected. The dimensions of these aggregates and the corresponding diffusion times are highly dependent on the ProtOG488/heparin ratio. The diffusion times of these aggregates vary in the range between 1000 and 2500 µs. This is near the region of typical diffusion times for polymersomes. Therefore, great care has to be taken if this method is applied to show whether heparin is bound to polymersomes. For unmodified polymersomes of 200 nm diameter, typical diffusion times of about 5700 µs were found (Tab. 1). It was also shown that heparin-polymersome-ProtOG488 conjugates have about double the diffusion times as compared to unfunctionalized polymersomes [47].

For further FCS analysis it was defined that only diffusion times slower than 2500 µs correspond to polymersomes. If the diffusion times were faster than this value, it was assumed that heparin-polymersome mixtures were not purified enough to ensure that there was no further free heparin present in the samples.

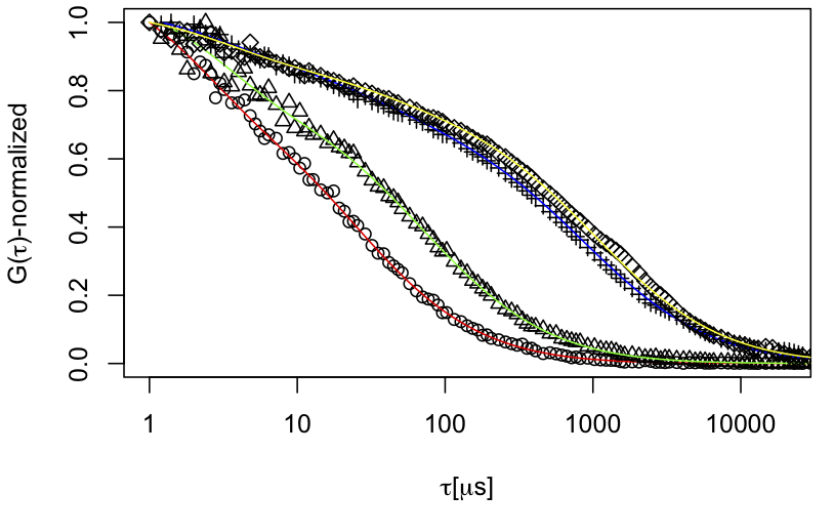

Figure 10: Normalized autocorrelation curves from FCS measurements with free OG488 in PBS (dots, red fit), free ProtOG488 (triangles, green fit), LMWH-ProtOG488 (crosses, blue fit), and heparin-ProtOG488 (squares, yellow fit).

The radial beam waist ω_{xy} for the argon laser at 488 nm excitation wavelength was calibrated by the measurement of free OG488 in PBS (Tab. 3) and the known absolute diffusion constant D = (4.11±0.06) x 10^{-6} cm^2 /s for OG488 [97]. This value is needed for the calculation of hydrodynamic radii R_H in the next chapters.

	Diffusion time τ_D [μs]	Diffusion constant D [cm^2/s] [97]	ω_{xy} [nm]
OG488 in PBS	23.6±1.7	(4.11±0.06) x 10^{-6}	197.0 ± 1.4

Table 3: Calibration of the radial beam waist ω_{xy} with the known diffusion constant D and the measured mean diffusion time of OG488 in PBS.

4.4 One-Pot Synthesis of Heparin-Polymersome Conjugates

One-pot synthesis was not successful, although there was no time for a broad investigation of different conditions. With naked eye detection by toluidine blue, there was never a color change found. This indicates that, if some heparin was bound to polymersomes, it was less than 16 μg/ml. With the protamine test, no polymersome fraction different from a negative sample was observed. Nevertheless, this approach seems to be promising and has to be evaluated further if this project is continued. Costs of such a preparation in particular would be much lower compared to the expensive linker system.

4.5 Synthesis of 2,6-Diaminopyridinyl Heparin

To introduce primary amino groups on the reducing ends of heparin, DAPH and DAPH-LMW were synthesized according to V. D. Nadkarni *et. al.* [87]. This step was necessary to obtain a readily accessible primary amino group on one side of the heparin chain, and that group can be further modified with amino reactive linkers or dyes. In solution, heparin is in an equilibrium state between the cyclic and the acyclic form at its reducing end. In the acyclic form the aldehyde can form an imine with one primary amino group of 2,6-DAP. Because this imine is not stable enough, it is best stabilized by its reduction to a secondary amine using sodium cyanoborohydride. The procedure is schematically represented below (Fig. 11).

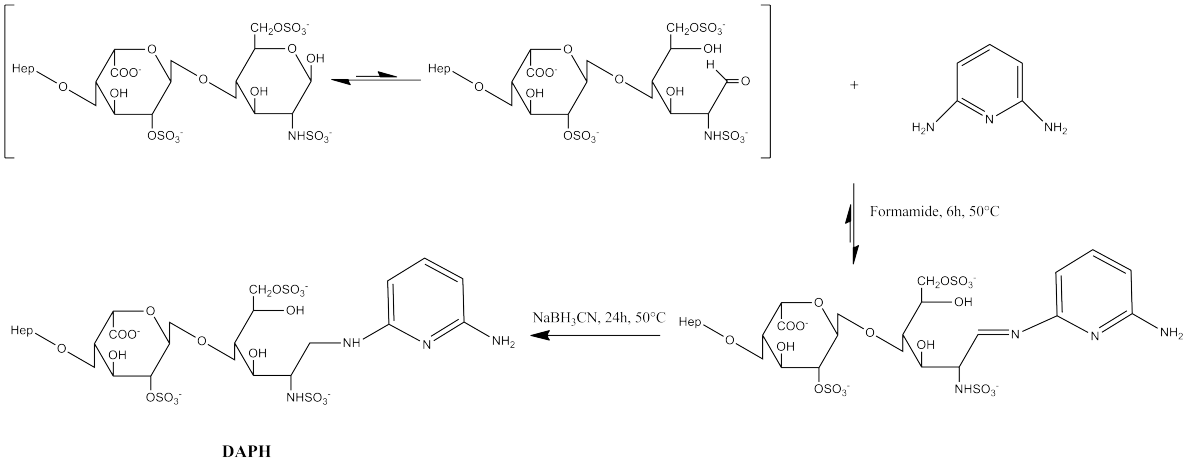

Figure 11: Schematic representation for the synthesis of DAPH and DAPH-LMW. Hep stands for the remaining chain in one heparin molecule.

The ^{1}H-NMR spectrum of LMWH (Appendix: Fig. 28) and of the final product DAPH-LMW after purification (Fig. 12) show the characteristic peaks for heparin: residue GlcNS(6S) δ 5.43 (br s, H-1), residue IdoA(2S) δ 5.24 (br s, H-1), residue GlcNS(6S/H) δ 3.29 (br s, H-2) and residue GlcNAc δ 2.06 (s, $COCH_3$). These peaks should appear at chemical shifts of 5.42±0.03 ppm, 5.21±0.03 ppm, 3.28±0.03 ppm, and 2.05±0.03 ppm, respectively [98].

Because 2,6-DAP should have reacted with the reducing end of heparin only, the 2,6-DAP concentration in the DAPH samples was very low and therefore difficult to detect by NMR. In order to see the characteristic peaks for 2,6-DAP, very high concentrations of DAPH had to be used. All of the recovered product was dissolved in at least 0.5 ml D_2O. The ^{1}H-NMR spectrum of DAPH looks similar, but the 2,6-DAP concentration was too low to see the peaks clearly (Appendix: Fig. 29). It was reported that the attached 2,6-DAP could be identified by a triplet at 7.39 ppm and a doublet at 6.09 ppm [87]. In our results the peaks were shifted to 7.64 ppm and 6.26 ppm. With the toluidine blue assay (standard curves Fig. 9) a recovery of 20% and 42% was calculated for heparin and LMWH, respectively. Compared to the reported recovery of 84% [87] for this synthesis with heparin, these yields are low, but for our purposes this is not crucial.

To derive the efficiency of this synthesis, the extinction coefficients of 2,6-DAP in conjugation

buffer pH 5.0 had to be determined first. From UV/Vis absorbance measurements of a concentration series of 2,6-DAP the extinction coefficients were calculated to ϵ_{240nm} = 8,593 M^{-1} cm^{-1} and ϵ_{333nm} = 13,810 M^{-1} cm^{-1}. The data for the linear fits were (240 nm, $y = 0.00959x + 0.01138$, R^2=0.9995) and (333 nm, $y = 0.01381x + 0.00789$, R^2=0.9997). 1 mg/ml DAPH or DAPH-LMW in conjugation buffer pH 5.0 were prepared. Subsequent UV/Vis absorbance measurements revealed 73% (DAPH) and 9% (DAPH-LMW) reaction efficiency, respectively.

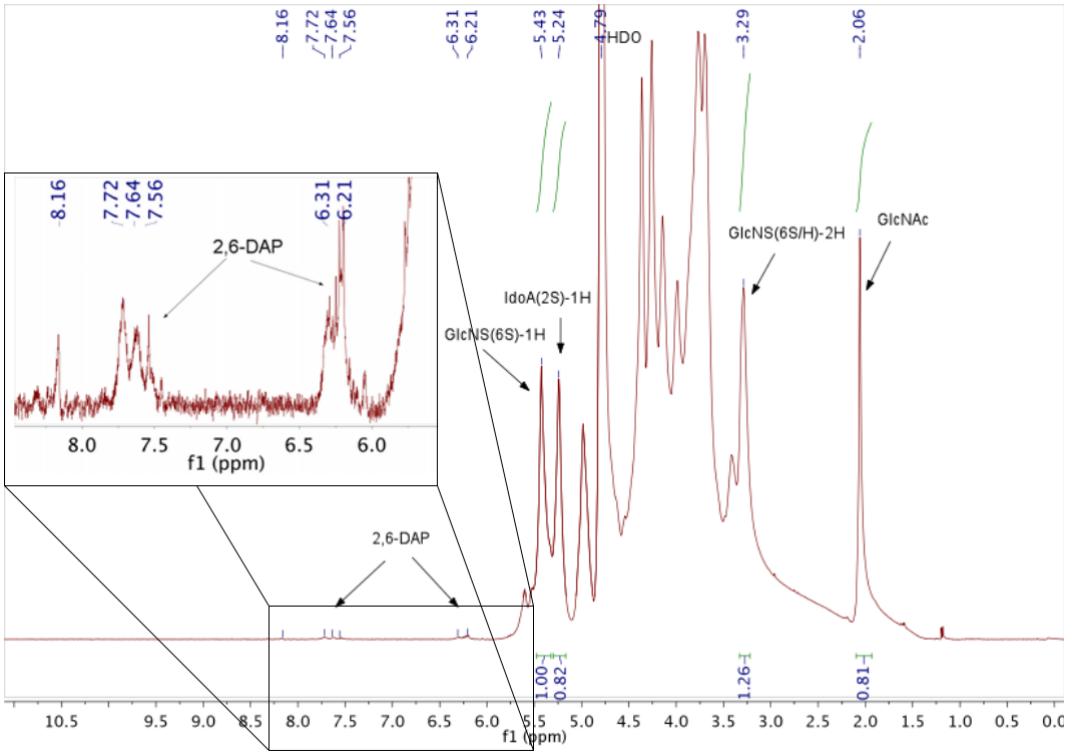

Figure 12: ^{1}H-NMR spectrum of 67 mg DAPH-LMW in 0.5 ml D_2O

With UV/Vis absorbance measurements the characteristic peaks for 2,6-DAP were verified in the DAPH (Fig. 16) and DAPH-LWH (Fig. 17) samples, including after additional purification with centrifugal filters. After DAPH-HyNic preparation the remaining residual 2,6-DAP would have been washed out during purification with centrifugal filters (MWCO = 3kDa or 10kDa). A solution of 10 mM 2,6-DAP in PBS was purified several times with centrifugal filters (MWCO = 10kDa) to test if residual 2,6-DAP can be washed out during purification. After 10 five-minutes centrifugations (13,400 RPM) no further 2,6-DAP was detectable in the retentate using UV/Vis absorption. Therefore, it was assumed that the peaks characteristic for aromatic protons in the ^{1}H-NMR spectra (Fig. 12, 29) come from 2,6-DAP bound at the reducing ends of heparin.

To check the availability of the newly attached primary amino group in DAPH, the coupling of OG488-NHS to heparin and DAPH was compared. After the SEC column, the fractions were recorded by UV/Vis absorbance at 493 nm for OG488 and 240 nm for 2,6-DAP. The first peaks, which correspond to OG-488-heparin conjugates, are shown below (Fig. 13). Comparison of the data from peak integration yields a 13-fold (240 nm, 2,6-DAP) and a 6-fold (493 nm, OG488) bigger peak area for

DAPH as compared to heparin. From these data it can be concluded that the naturally occurring amino groups on heparin can partially react with OG488-NHS but the remaining primary amino group of 2,6-DAP in DAPH couples much more efficiently. The fact that the peak at the specific absorbance of 2,6-DAP (240 nm) is much bigger for DAPH than for heparin gives further evidence that 2,6-DAP in DAPH and DAPH-LMW were bound covalently to heparin. Otherwise 2,6-DAP-OG488 would have resulted, which would not have eluted in the same fraction as the sugars. Heparin was verified with a toluidine blue assay of the fractions of the first peaks.

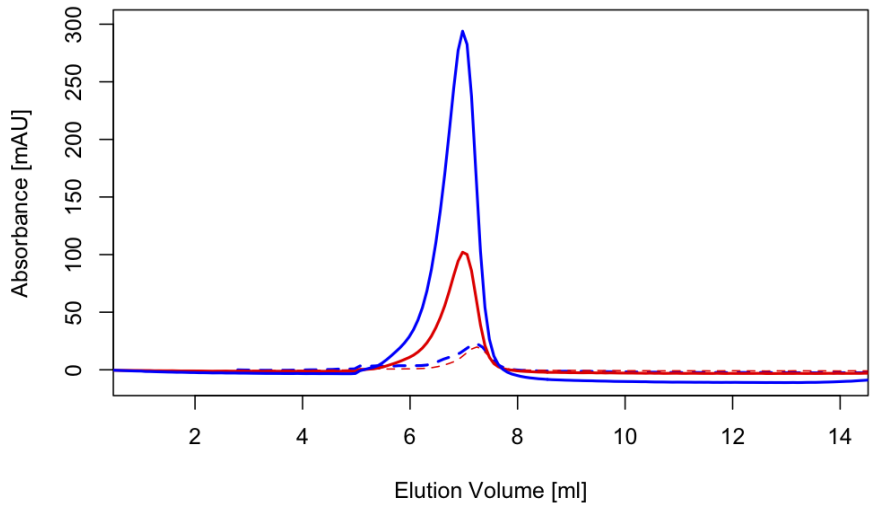

Figure 13: Size exclusion chromatography of OG488 labelled DAPH (solid lines) and heparin (dashed lines) on Sephadex G25 column in PBS. The red curves show the absorbance for OG488 at 493 nm, the blue curves the absorbance of 2,6-DAP at 240 nm.

The products were further analyzed by diffusion measurements with FCS (Tab. 4, Fig. 14). The second diffusion times for DAPH-OG488 and heparin-OG488 were similar, but in the second sample more free OG488 was present. The count rate for DAPH-OG488 was higher by a factor of 12 than for heparin-OG488, when the count rate was multiplied by % of the second fraction. In summary, this means that OG488-NHS can couple to DAPH with higher efficiency than to heparin.

	OG488	DAPH-OG488	Heparin-OG488
Diffusion time τ_D 1st Fraction [µs]	-	28.2 fixed	28.2 fixed
1st Fraction [%]	-	40	75
Diffusion time τ_D 2nd Fraction [µs]	28.2±0.4	187±29	166±26
2nd Fraction [%]	100	60	25
R_H 2nd Fraction [nm]	0.60±0.01	4.0±0.6	3.6±0.6

Table 4: Diffusion time τ_D and R_H from FCS measurements of free OG488, DAPH-OG488, and heparin-OG488 in PBS.

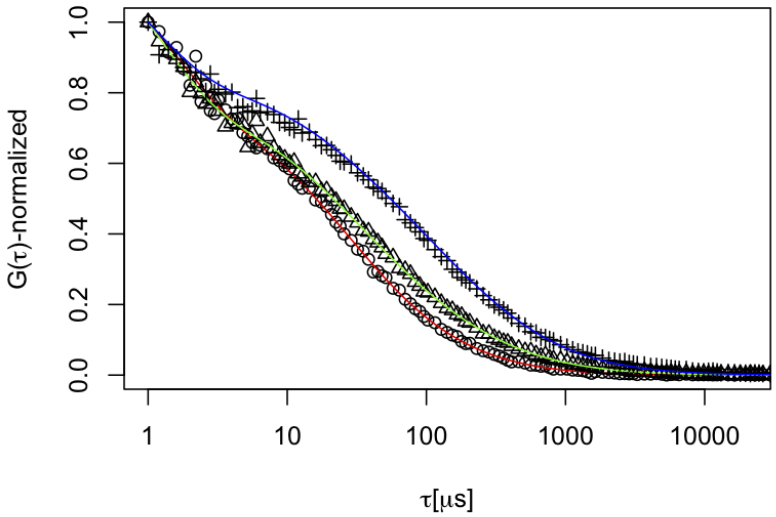

Figure 14: Normalized autocorrelation curves from FCS measurements with free OG488 in PBS (dots, red fit), heparin-OG488 (triangles, green fit), and DAPH-OG488 (crosses, blue fit).

It can be concluded that 2,6-DAP was successfully coupled to the reducing end of heparin, although the yields were low. The product DAPH shows better coupling of OG-488-NHS than heparin. It means that the remaining primary amino group of 2,6-DAP is available and can react with succinimidyl esters. Heparin itself can also react with succinimidyl esters, but much less efficiently. Most of the amino groups in heparin are not well accessible. It can be assumed that further modification with Sulfo-S-HyNic happens preferentially on the 2,6-DAP moiety of DAPH, less on natural amino groups in heparin. This ensures that subsequent coupling to polymersomes results in heparin-polymersome conjugates with the heparin attached at one point only, namely at its reducing end. This is the natural form of heparin when it is coupled to a substrate.

4.6 Modification of DAPH

It was shown that the newly attached primary amino group in DAPH can react with amino reactive succinimidyl esters (Fig. 13, 14). This concept was now applied to couple the sulfo-succinimidyl-6-hydrazinonicotinate acetone hydrazone (Sulfo-S-HyNic) linker to DAPH. The reaction schema is presented below (Fig. 15). Of the 60 monomers in heparin, only 12 are modeled in the picture. Conformation data from Ref. [99] were used for this drawing.

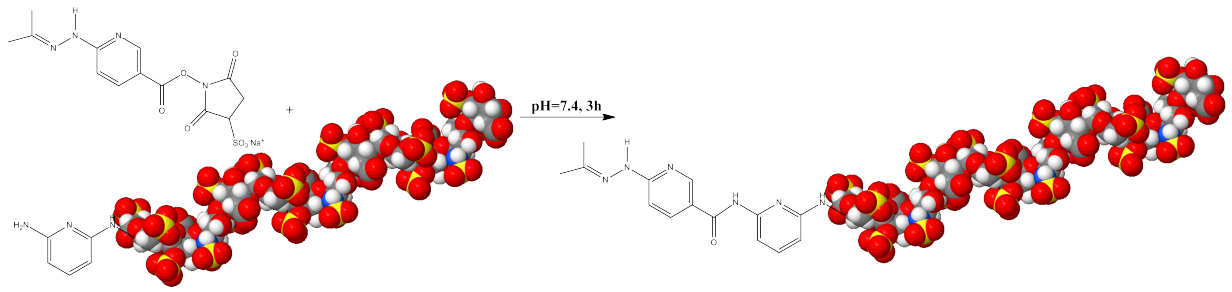

Figure 15: Schematic representation of the reaction between DAPH and Sulfo-S-HyNic. The actual heparin would be 48 monomers longer on average. For heparin, 100% Van der Waals radii are presented for each atom in the following colors: C (gray), H (white), O (red), S (yellow), and N (blue).

The reaction of Sulfo-S-HyNic with DAPH is highly dependent on the concentration of DAPH and the excess of Sulfo-S-HyNic. Several different conditions were tested until the optimal mixture was found. Normally, the DMSO concentration should be kept under 5% (v/v) [100]. This is critical if proteins are used. In our case, whether DAPH precipitates at higher DMSO concentrations was tested. But up to 50% (v/v) DMSO there was no precipitation observable. Also, the sugar concentration (15 mg/ml) in the reaction mixtures was required to be very high compared to the reported protein concentrations (2 mg/ml). One reason for the need for these high concentrations of sugars and high excesses of Sulfo-S-HyNic is the low concentration of accessible primary amino groups on DAPH compared to proteins. Furthermore, the hydrolysis of the succinimidyl ester of Sulfo-S-HyNic competes with the reaction with primary amino groups. This makes the concentration of biomolecules to be modified and the excess of linker critical parameters for a successful reaction.

On the other hand, there was also a possibility that DAPH-HyNic reacted with the unmodified reducing ends of heparin, these still being present in the solution [101]. But at the reducing end of heparin there is a non-aromatic aldehyde, the hydrazone bond with this aldehyde would be less stable. Furthermore, the hydrazine group on the HyNic moiety was protected in the form of its acetone hydrazone and coupling to aldehydes happens only under mild acidic conditions up to pH 7.3 [102]. The purification steps for DAPH-HyNic were performed in modification buffer pH 7.4 and, when expedient, the buffer was exchanged for conjugation buffer pH 6.0 in the last purification steps only. This ensured that DAPH-HyNic was only active if the aromatic aldehydes on the polymersomes were already present in the mixture. The probability of undesirable DAPH-HyNic-heparin complex formation was very low, because only 26% of heparin in DAPH did not have a 2,6-DAP group at its reducing ends. Finally, only the coupling of HyNic with an aromatic aldehyde gives the specific UV/Vis absorbance band at 380 nm.

The reaction was also performed with the more hydrophobic linker S-HyNic. But here precipitation was observed during the reaction under the same conditions as for Sulfo-S-HyNic. If only the leaving group had precipitated after the reaction, no effect on the yield of final DAPH-HyNic product should have been observed. But when precipitation was observed there was always a very low yield of coupling product found.

To test if HyNic was successfully bound to DAPH and if they were accessible, the samples were

mixed with a 4-NB solution. This is an analog to 4-FB which is the linker on the polymersomes which should form the bis-aryl hydrazone bond with the HyNic linker. The reaction between HyNic and 4-NB leads to a bis-aryl hydrazone bond with a specific absorbance at 380 nm (ϵ=22,000) [102].

This specific absorbance of the reaction product between DAPH-HyNic and 4-NB is shown in the following figure (Fig. 16). The two peaks at 240 nm and 333 nm correspond to the 2,6-DAP moiety on DAPH (blue curve). In the reaction product the specific absorbance at 380 nm (red curve) is clearly visible. This rules out forming an undesired DAPH-HyNic-heparin complex at a significant concentration. The additional peak at 300 nm comes from the HyNic group. The green curve represents the mixture of the rest of the last diafiltration step with 4-NB. This shows that the purification was successful; no further free HyNic was present in the sample. The yield of DAPH-HyNic can be estimated using the known and calculated extinction coefficients. Typically, about 76% of DAPH was left after purification and, of that, 52% was successfully coupled to HyNic, whereas these HyNic groups were also reactive. When started with 1 mg of DAPH sample, 0.29 mg DAPH-HyNic were obtained. For 1 ml polymersome solution a maximum of 20 µg DAPH-HyNic can be coupled to 4-FB on the polymersomes (Section 4.8). The actual yield resulted in at least a 10-fold excess of DAPH-HyNic over accessible 4-FB in each conjugation sample.

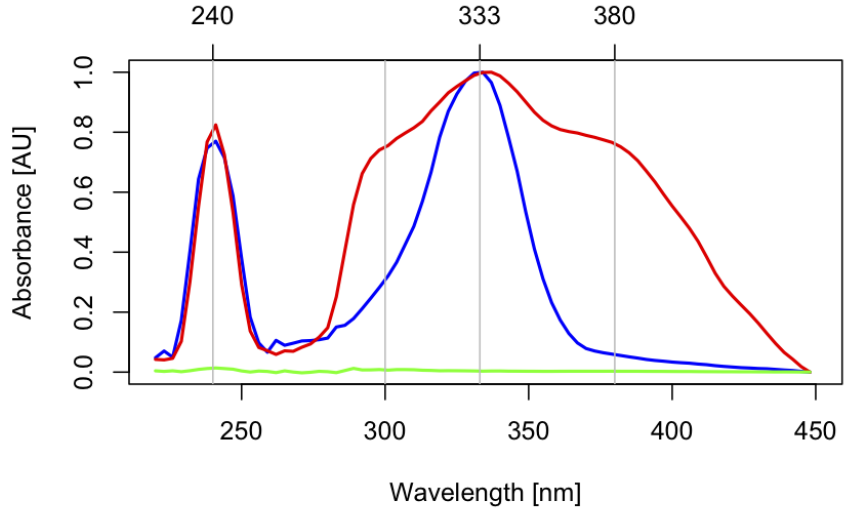

Figure 16: Normalized UV/Vis absorption spectra of DAPH (blue), DAPH-HyNic-4-NB conjugates (red) and a control (green) in conjugation buffer pH 5.0. The vertical grey lines mark the wavelengths specific for 2,6-DAP (240 nm, 333 nm), HyNic (300 nm), and the bis-aryl hydrazone bond formed between HyNic and 4-NB (380 nm).

The same curves, as shown before, are presented for DAPH-LMW when different Sulfo-S-HyNic excesses were used (Fig. 17). The yield of coupling products (380 nm) compared to 2,6-DAP (333 nm) was always lower for DAPH-LMW than for DAPH. One reason is that only 8.6% of LMWH had a 2,6-DAP at its reducing end. This increased the possibility that the hydrazine on HyNic reacted with free reducing ends of LMWH.

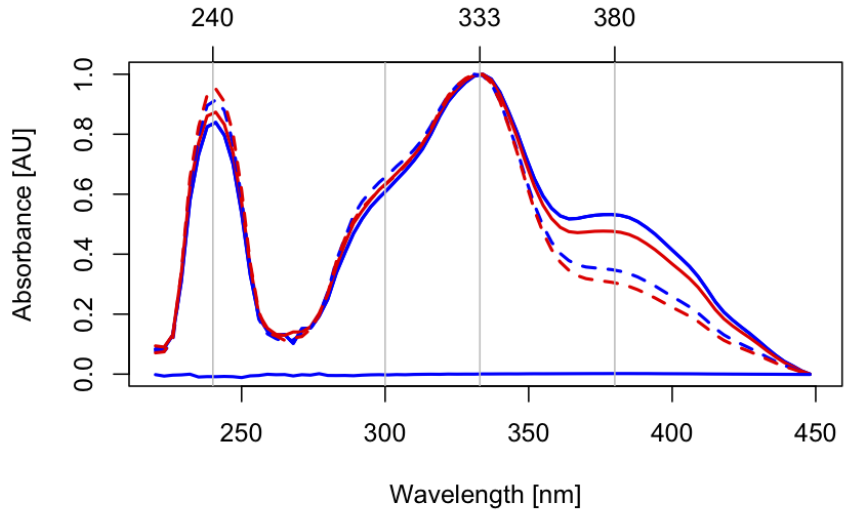

Figure 17: Normalized UV/Vis absorption spectra of DAPH-LMW-HyNic-4-NB conjugates and a control (green) in conjugation buffer pH 5.0. Different excesses of Sulfo-S-HyNic over DAPH-LMW were used to produce DAPH-LMW-HyNic conjugates. The following excesses of Sulfo-S-HyNic over DAPH-LMW were used: 53 (solid blue), 35 (solid red), 18 (dashed blue), 9 (dashed red). The vertical grey lines mark the wavelengths specific for 2,6-DAP (240 nm, 333 nm), HyNic (300 nm), and the bis-aryl hydrazone bond formed between HyNic and 4-NB (380 nm).

4.7 Modification of Polymersomes

To functionalize polymersomes with the counterpart of HyNic (aromatic aldehyde), Sulfo-S-4FB or PEG_4PFB were reacted with polymersomes in modification buffer pH 8.3 (3 mg/ml, AB-NH 5%). When the linker, which was dissolved in DMSO, was added directly to polymersome solutions, the polymersomes dissolved. Therefore, it was necessary to put the linkers in buffer first, and then this mixture was added to the polymersome solutions. The schematic procedure for the PEG_4PFB linkers is presented in the following figure 18.

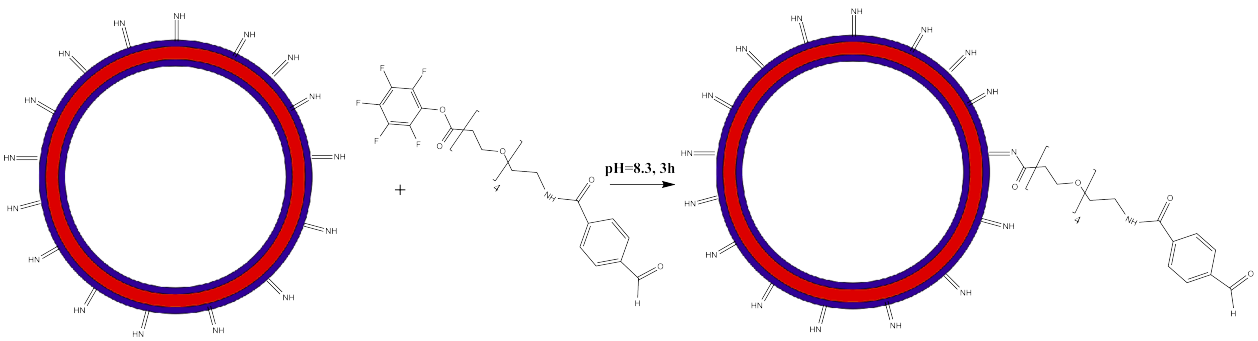

Figure 18: Schematic representation of the modification of polymersomes with PEG_4PFB linkers. The hydrophobic part of the polymer bilayer is drawn in red, the hydrophilic part in blue.

Modification of polymersomes to obtain 4-FB moieties on the surfaces was found to be a crucial step. It was reported that S-4FB can couple successfully to exactly the same polymersomes as used

here [65, 103]. Furthermore, it was claimed that HyNic-modified eYFP and antibodies can form a bis-aryl hydrazone bond with the 4-FB moieties on the polymersomes. This bond exhibits a specific UV absorbance at 354 nm (ϵ_{354nm} = 29,000 M^{-1} cm^{-1} [100]). But this absorption band has never been shown in a final product. The coupling was verified indirectly by FCS, laser scanning microscopy and specific cellular uptake by SKBR3 cells [65]. But if these proteins are able to bind nonspecifically to the polymersomes, the same results would have been obtained using the mentioned methods. In such a case it would not be possible to distinguish between specific and nonspecific binding.

To test the two different available linkers for polymersome modification, V-4FB and V-PEG4FB were reacted with 2-HyPy. This should have resulted in a bis-aryl hydrazone bond with a specific absorption at 350 nm (ϵ_{350nm} = 18,000 M^{-1} cm^{-1} [100]). After purification, UV/Vis absorbance measurements were recorded before lyophilization in water and after lyophilization in 150 µl ethanol (Fig. 19). Theoretical polymer concentrations were 3.3 mg/ml in water (0.5 mM) or 32.0 mg/ml in ethanol (5.2 mM). Before lyophilization, light scattering by the polymersomes prevented the specific absorbances at 354 nm from appearing. By subtracting a standard polymersome solution, the peaks became visible (Fig. 19). In water, the theoretical concentration of AB-NH in the outer layer of the polymersome membranes was 13.4 µM. Using the extinction coefficient of the bis-aryl hydrazone bond, concentrations of the successfully coupled product were 1.4 µM (V-4FB) and 8.2 µM (V-PEG4FB), respectively. In ethanol, the polymer concentrations were a factor of six higher than in water. For V-PEG4FB-HyPy the peak at 350 nm was bigger in ethanol, as expected, whereas for V-4FB-HyPy it did not change much. Furthermore, the peak for V-4FB-HyPy in water appears at 340 nm, which is 10 nm away from the reported value. These two observations give rise to doubt that Sulfo-S-4FB is a suitable linker.

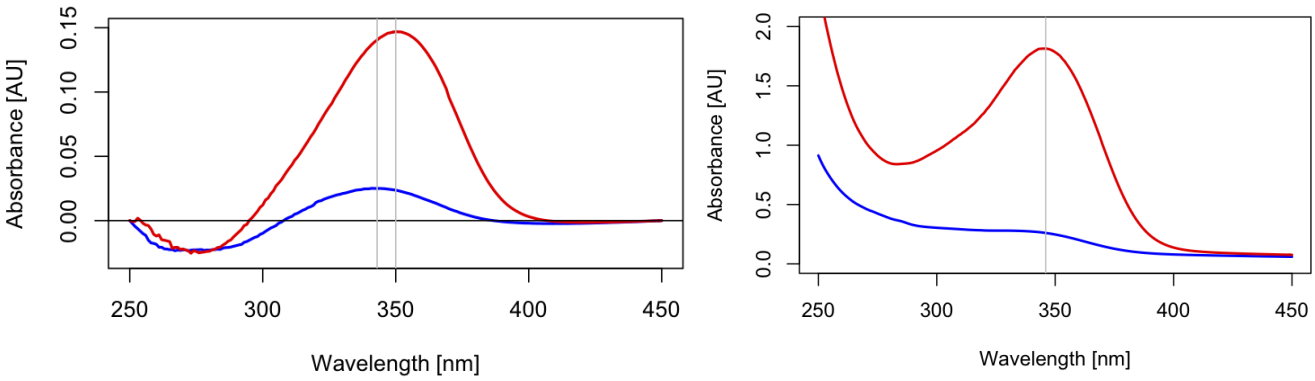

Figure 19: UV/Vis absorption measurements of polymersome-linker-HyPy conjugates. Polymersome-PEG_4-4FB-HyPy are shown in red, polymersome-4FB-HyPy are drawn in blue. Left: UV/Vis absorption before lyophilization in water after subtraction of a standard polymersome solution (grey lines: 341 nm, 350 nm). Right: UV/Vis absorption after lyophilization in ethanol (grey line: 346 nm).

These data show clearly that the coupling reaction works better with PEG_4-PFB linkers than with Sulfo-S-4FB linkers. In the case of Sulfo-S-4FB, either the coupling to the polymersomes was not successful enough or most of the aldehydes are not accessible to form a bis-aryl hydrazone bond with 2-HyPy. It is even possible that Sulfo-S-4FB did not react at all with the polymersomes, and the low peaks (blue) in the figure came from free 4-FB-HyPy conjugates. Control experiments with linker and 2-HyPy mixtures, after the same purification steps, also showed low peaks at about 350 nm [103]. The UV/Vis absorbance of V-4FB-HyPy shown in figure S4 b (Supp. Info. Ref. [65]) were obtained with the PEG_4-PFB linker, not with Sulfo-S-4FB. But all other experiments in this reference were carried out with Sulfo-S-4FB. These problems will be discussed further in the next sections.

4.8 Coupling of DAPH to Polymersomes

The formation of the bis-aryl hydrazone bond between DAPH-HyNic and V-4FB or V-PEG4FB should proceed at pH 5.0 or 6.0. The reaction scheme is given below (Fig. 20). The final coupling products are abbreviated as V-DAPH.

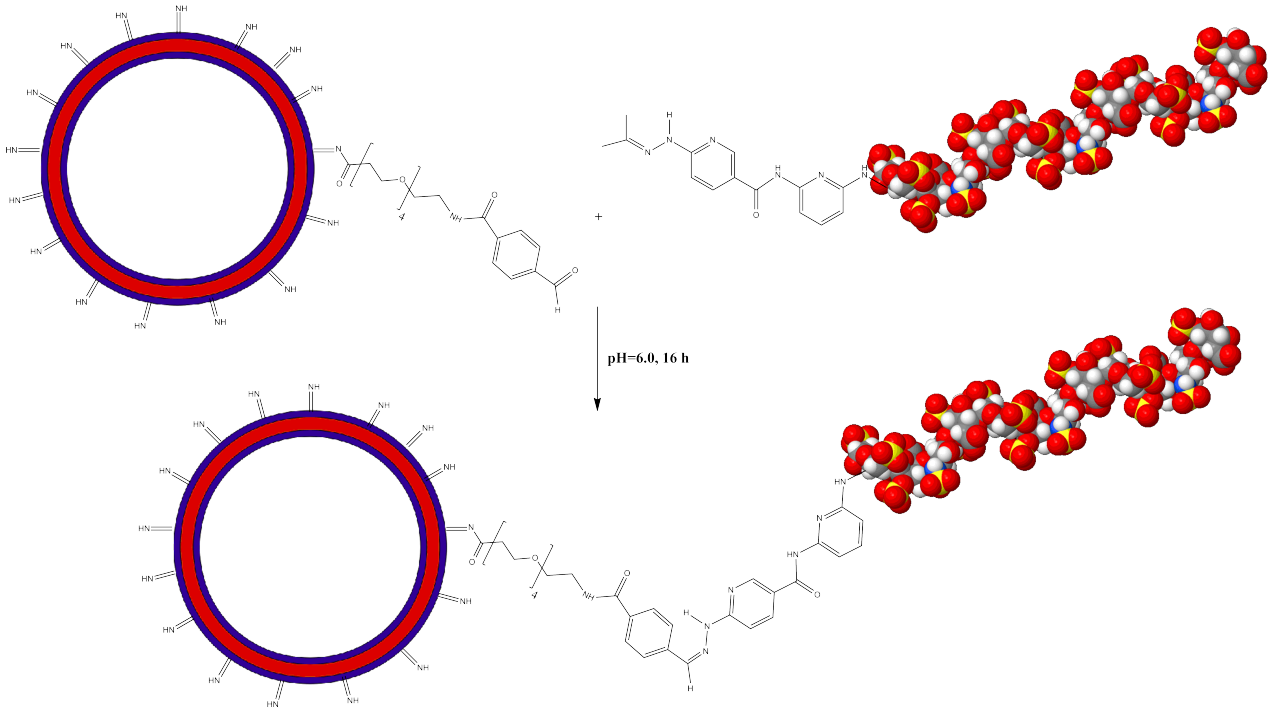

Figure 20: Schematic representation of the conjugation reaction between DAPH-HyNic and V-PEG4FB forming a stable bis-aryl hydrazone bond.

A rough estimation of the theoretically possible concentration of heparin coupled to polymersomes (3 mg/ml polymer, 5% AB-NH) was calculated using the reported efficiency of 10% [65]. In such a sample, about 1.2 µM AB-NH should be accessible for the coupling of heparin. This would lead to a theoretical concentration of 22 µg/ml in case of DAPH or 6 µg/ml for DAPH-LMW. This reveals the problems with the toluidine blue assay. To detect heparin with this method, the samples should contain at least 16 µg/ml heparin or 20 µg/ml LMWH. When extensive dialysis (MWCO = 300 kDa)

was used for purification, the V-DAPH samples contained detectable heparin concentrations in some cases. Therefore, it was first assumed that the conjugation reaction worked properly. But it turned that these mixtures were not purified successfully from free heparin. This conclusion was drawn because the fits from the protamine test showed only diffusion times faster than 2500 µs. Whereas TEM pictures (Appendix: Fig. 30), after the coupling reaction, did not show any decrease in vesicle diameter.

It was decided to purify the samples by FPLC on a Superdex 200 10/300 GL column in PBS. Here, heparin was detected in the polymersome fraction. Again, successful coupling was assumed. But later on, it was found that free heparin also eluted in the polymersome fraction. This means that the exclusion limit of Superdex 200 10/300 GL was too low (100 kDa for dextrans). Free heparin could not enter the matrix and did not elute in retarded fashion as compared to the polymersomes.

Therefore, the column was changed to Sepharose 2B. The exclusion limits of a Superdex 200 10/300 GL column and a Sepharose 2B column are 1.3 x 10^6 Da and 40 x 10^6 Da for globular proteins, respectively. The Sepharose 2B column was found to be the only satisfying purification method, to separate V-DAPH from free heparin. But after this purification, heparin was never detected in a polymersome fraction by toluidine blue. In some cases, the polymersome fraction was concentrated 10-fold and still no heparin was detectable. This indicates that the concentration was definitely lower than 16 µg/ml for heparin or 20 µg/ml for LMWH.

UV/Vis absorbance detection of the bis-aryl hydrazone bond (ϵ_{354nm} = 29,000 M^{-1} cm^{-1} [100]) was difficult, because polymersomes scatter light at these wavelengths. The peaks were extracted by subtracting a V-NH reference sample in PBS. Fig. 21 represents UV/Vis absorbance measurements of V-PEG4FB-HyPy (from Fig. 15, red), V-PEG4FB-DAPH (blue, solid line) and V-PEG4FB-DAPH after an additional four days incubation time (blue, dashed line) in PBS. The absorbance of a V-NH reference sample in PBS was subtracted. For the dashed line, the concentration of V-DAPH was determined to 828 nM, which corresponds to 15 µg/ml heparin, which is exactly at the limit of resolution for the toluidine blue assay. But it is doubtful that these data are useful for quantification and must be handled with care.

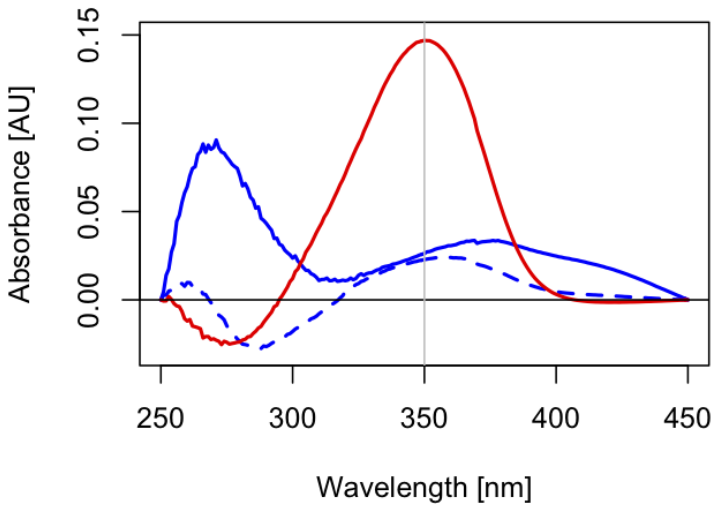

Figure 21: Normalized UV/Vis absorption spectra of V-PEG4FB-HyPy (from Fig. 19, red), V-PEG4FB-DAPH (blue, solid line) and V-PEG4FB-DAPH after additional 4 days incubation time (blue, dashed line) in PBS. All data are represented after subtraction of absorbance of a V-NH reference sample in PBS.

As seen previously (Sect. 4.7), V-PEG4FB can form a detectable bis-aryl hydrazone bond with 2-HyPy. The reaction between V-PEG4FB and DAPH is much less efficient, as visible by the smaller peaks at 350 nm. Of course, heparin is a much bigger molecule with many negative charges. Therefore, steric hindrance is one reason for the lower coupling efficiency for DAPH compared to 2-HyPy. The maxima of the blue curves do not correspond very well to the red curve. Final conclusions about the success of the coupling reaction are difficult. A protamine test and an antibody test were performed to further check the presence of heparin-polymersome conjugates.

4.8.1 Protamine Test

After polymersomes and ProtOG488 were mixed, the FCS measurements were performed without (Tab. 5, Fig. 22) or with (Tab. 6, Fig. 23) additional SEC on Sepharose 2B. For V-NH and V-PEG4FB without SEC there was no significant polymersome fraction measured by FCS. Although some very bright peaks were observed (six single peaks in 3 x 10 measurements) in the V-PEG4FB ProtOG488 mixture. The measurements containing these peaks were excluded from the fit, because these six very bright peaks would give rise to a disproportional fraction of a slow diffusing species.

Sometimes, these negative controls showed a significant, slowly diffusing species, which could correspond to polymersomes. This provided some evidence that proteins can bind nonspecifically to V-NH or V-PEG4FB. This would make the detection by FCS very difficult. The specific reaction between V-PEG4FB and DAPH would not be evaluable. In any case, V-DAPH often appeared different as compared to the negative samples. Some evidence for the presence of heparin on the polymersome surfaces in V-DAPH comes from the fit values (Tab. 5). Whereas there was always a fraction of free

ProtOG488 detected in the negative samples, this was not the case for V-DAPH. In the V-DAPH ProtOG488 mixture, the fast-diffusing species was free OG488. Because there was already free OG488 measurable in the ProtOG488 sample, it can be assumed that nearly all of the ProtOG488 was bound to V-DAPH. Furthermore, the hydrodynamic radius R_H for V-DAPH-ProtOG488 was about a factor 1.5 bigger as compared to non-functionalized polymersomes (Tab. 1). This has already been reported for heparin-polymersome conjugates, and for ProtOG488 as fluorescent probes [47].

	ProtOG488	V-NH	V-PEG4FB	V-DAPH
Diffusion time τ_D 1st Fraction [µs]	21.4 fixed	21.4 fixed	21.4 fixed	21.4 fixed
1st Fraction [%]	55	73	68	65
Diffusion time τ_D 2nd Fraction [µs]	90	90 fixed	90 fixed	90 fixed
2nd Fraction [%]	45	15	30	0
Diffusion time τ_D 3rd Fraction [µs]	-	3052±1811	5374±2745	8849±1021
3rd Fraction [%]	-	12	2	35
R_H 3rd Fraction [nm]	1.9	65±39	115±59	190±22

Table 5: Diffusion time τ_D and R_H from FCS measurements of free ProtOG488, V-NH-ProtOG488, V-PEG4FB-ProtOG488, and V-DAPH-ProtOG488 in PBS.

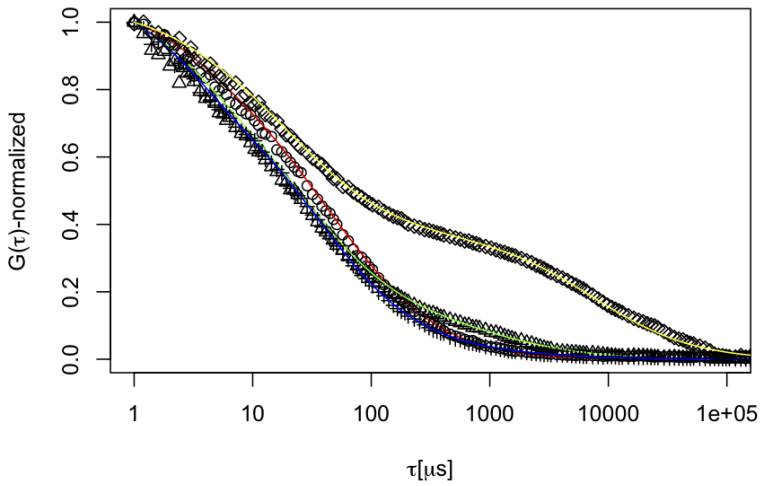

Figure 22: Normalized autocorrelation curves from FCS measurements with free ProtOG488 in PBS (dots, red fit), V-NH-ProtOG488 (triangles, green fit),V-PEG4FB-ProtOG488 (crosses, blue fit), and V-DAPH-ProtOG488 (squares, yellow fit).

When the protamine test was performed with additional SEC, the difference between V-DAPH and the negative samples vanished (Tab. 6, Fig. 23). This means that ProtOG488 also binds non-specifically to V-NH polymersomes. The difference in diffusion times between positive and negative samples was not significant.

	ProtOG488	V-PEG4FB	V-DAPH
Diffusion time τ_D 1st Fraction [µs]	24.4 fixed	86 fixed	86 fixed
1st Fraction [%]	50	34	25
Diffusion time τ_D 2nd Fraction [µs]	86	4267± 1772	4813±757
2nd Fraction [%]	50	66	75
R_H 2nd Fraction [nm]	1.8	91±38	103±16

Table 6: Diffusion time τ_D and R_H from FCS measurements of free ProtOG488, V-PEG4FB-ProtOG488, and V-DAPH-ProtOG488 in PBS after purification with SEC.

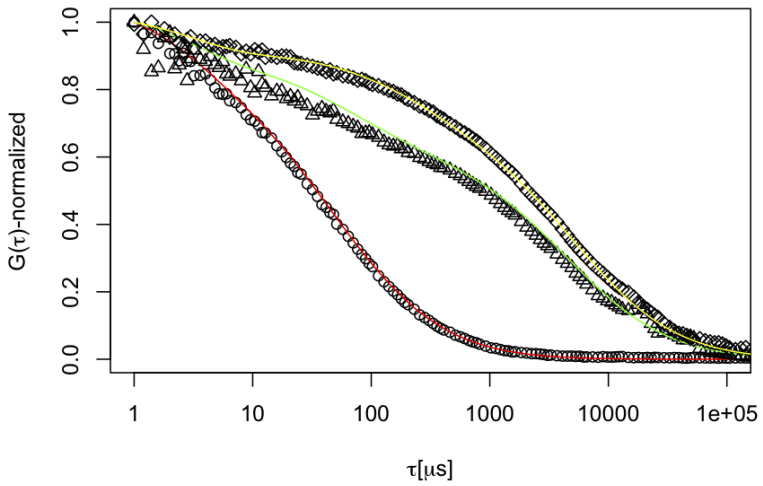

Figure 23: Normalized autocorrelation curves from FCS measurements with free ProtOG488 in PBS (dots, red fit), V-NH-ProtOG488 (triangles, green fit), and V-DAPH-ProtOG488 (squares, yellow fit) after purification with SEC.

4.8.2 Antibody Test

Another method to detect successful coupling of heparin to polymersomes was similar to the protamine test. But here, the probe protein was an OG488-labeled anti-heparin antibody (AbHepOG488). Without separation of unbound AbHepOG488 and AbHepOG488-polymersome conjugates, it was not possible to detect any slowly diffusing species, which would correspond to polymersomes. Therefore, after mixing polymersome solutions with AbHepOG488 solutions and three hours of incubation, additional SEC was performed. The FCS measurements after purification are shown below (Fig. 24).

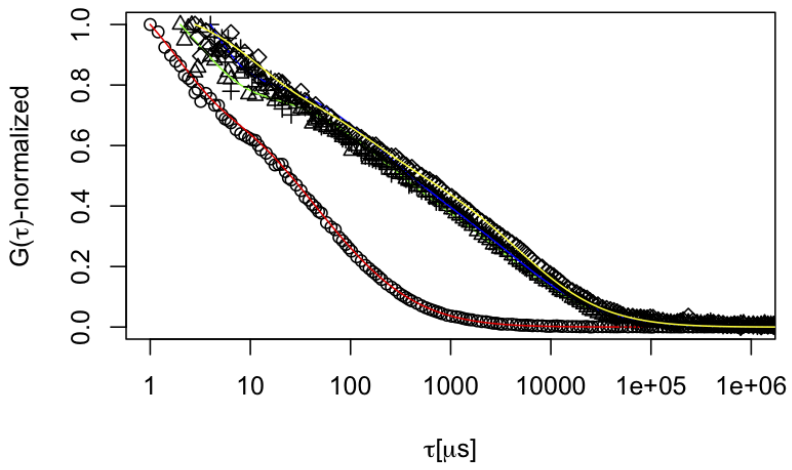

Figure 24: Normalized autocorrelation curves from FCS measurements with free AbHepOG488 in PBS (dots, red fit), V-NH-AbHepOG488 (triangles, green fit),V-PEG4FB-AbHepOG488 (crosses, blue fit), and V-DAPH-AbHepOG488 (squares, yellow fit).

Again, the results look the same for positive and negative samples. A fraction of about 53% with a diffusion time τ_D = (4718±824) µs was found in each sample. This means, that antibodies also bind nonspecifically to polymersomes with 5% AB-NH or PEG4FB moieties. This test seems to be unsuitable to verify whether heparin successfully couples to polymersomes or not. Furthermore, it gives more evidence to doubt the results of Ref. [65]. More precisely, their methods to test successful specific binding of biomolecules to polymersomes with the SoluLink chemistry were not suitable. Their results for polymersome-antibody- and polymersome-eYFP conjugates could have been obtained with nonspecific binding alone. It can be speculated that Alexa 647-M-containing polymersomes with nonspecifically attached anti-biotin IgGs would recognize the biotin pattern (Fig. 4, Ref. [65]) as well.

This hypothesis was tested further by repeating the eYFP coupling to polymersomes (Sect. 4.9) reported in the same reference [65]. In particular, nonspecific binding of eYFP to V-NH was analyzed again, because in Ref. [65, 103] only one negative measurement, which checks for nonspecific binding, was performed.

Another reason that polymersome fractions were found in all of the samples (also in the protamine test Fig. 23) could have been that free OG488, which was always present in ProtOG488 or AbHepOG488 solutions, bound nonspecifically to the polymersomes, and not to the labeled proteins. Therefore, a similar test was carried out with OG488 alone. A V-NH polymersome solution was mixed with free OG488 in PBS, incubated for three hours and purified by SEC. The resulting FCS measurements of the polymersome fraction showed a very low signal, with diffusion times corresponding to freely diffusing OG488 only. Therefore, it can be concluded that really the labeled proteins were bound to the polymersomes, not to free OG488.

4.9 Coupling of eYFP to Polymersomes

Because several problems were observed with the linker system, one experiment from the reference [65] was repeated. To control the linker availability on the vesicles, HyNic-eYFP was coupled to V-PEG4FB (V-PEG4FB-eYFP). As a negative control HyNic-eYFP was added to non-functionalized vesicles V-NH (V-NH-eYFP, 5% AB-NH). After the conjugation reaction, SEC was performed to separate free eYFP and eYFP-conjugated polymersomes. The following graph (Fig. 25) shows FCS curves for free eYFP (red fit), V-PEG4FB-eYFP (green fit), and V-NH-eYFP (blue fit).

The curves for positive and negative control look roughly the same. Only some differences in counts per molecule (CPM) were observed. For the positive control, the CPM was about four times larger than for the negative samples. From these data no conclusions can be drawn as to whether HyNic-eYFP was conjugated via the linker or whether it was only bound nonspecifically to the polymersomes. To rely only on the difference in CPM is critical, because it is also known that nonspecific binding can influence the stability of fluorescent proteins [104].

The reason why this negative sample looks different from Ref. [65] could be that, here, HyNic-eYFP was used for the negative samples, whereas unmodified eYFP was used in the cited paper. HyNic moieties are hydrophobic, as reported by the manufacturer [100, 101]. Therefore, it is possible that the hydrophobic HyNic group on eYFP was incorporated into the hydrophobic part of the polymer membrane, anchoring the protein to the polymersomes.

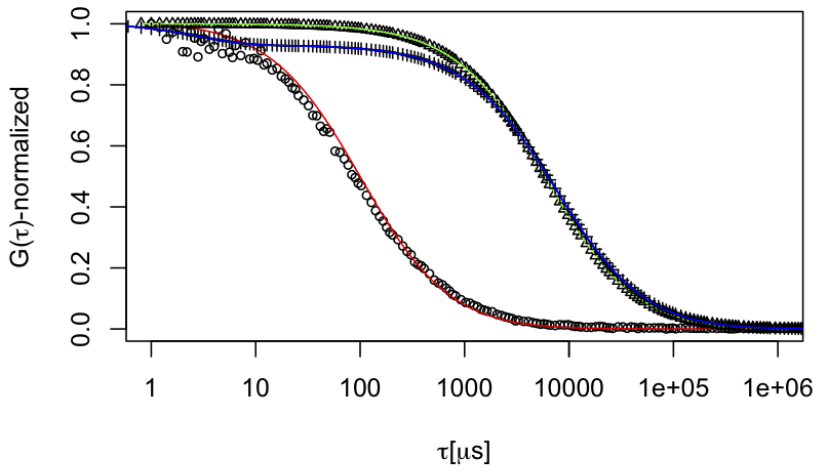

Figure 25: Normalized autocorrelation curves from FCS measurements with free eYFP in PBS (dots, red fit), V-PEG4FB-eYFP (triangles, green fit), and a negative control with V-NH-eYFP (crosses, blue fit).

	eYFP	V-PFB-eYFP	V-NH-eYFP
Diffusion time τ_D [µs]	100±2	6080±460	6750±740
CPM [kHz]	7.5±0.1	370±96	103±37
R_H [nm]	2.1±0.1	130±10	145±16

Table 7: Diffusion time, CPM, and R_H from FCS measurements of free eYFP in PBS, V-PFB-eYFP, and V-NH-eYFP conjugates.

UV/Vis-absorption measurements were recorded for both samples. As a reference, vesicles without eYFP (5% AB-NH) were measured and subtracted from the sample data (Fig. 26). Two maxima were found at positions 356 nm and 516 nm. The peak at 516 nm clearly corresponds to eYFP (ϵ_{514nm} = 84,000 M^{-1} cm^{-1} [105]). The peak at 356 nm reflects either the absorbance of the bis-aryl hydrazone bond (ϵ_{354nm} = 29,000 M^{-1} cm^{-1} [100]), or also absorbance of eYFP. It was reported that the eYFP excitation overlaps with the specific absorbance of the bis-aryl hydrazone bond at 354 nm [103]. From our data, no clear conclusions can be drawn. Firstly, there should be a peak at 280 nm, because eYFP contains tryptophan. Secondly, if the peak at 356 nm corresponded to the absorbance of the bis-aryl hydrazone bond, it should be smaller than the peak at 516 nm, because the extinction coefficient is a factor of three smaller for the bis-aryl hydrazone bond than for eYFP at 514 nm. Thirdly, the peak at 356 nm also appeared in the negative sample, where no such bond was possible.

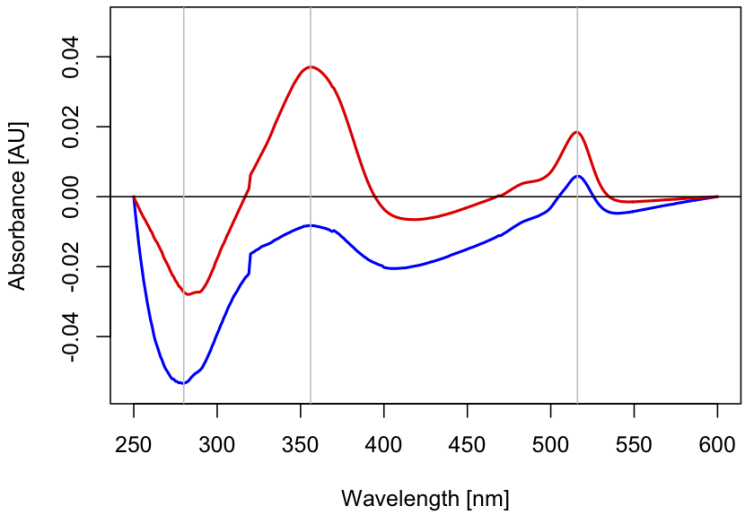

Figure 26: Normalized UV/Vis absorption spectra of PEG_4PFB-vesicles-eYFP (positive, red), NH-vesicles-eYFP (negative, blue), after subtraction of absorbance of a NH-vesicle in PBS reference sample. Vertical grey lines mark the wavelengths 280 nm, 356 nm , and 516 nm respectively.

In summary, it is difficult to use fluorescent proteins and FCS to test whether a desired molecule coupled to polymersomes by a specific bond. More experiments are necessary to draw final conclusions as to which linkers are suitable and which not. Importantly, the observed nonspecific binding of fluorescent proteins (ProtOG488, AbHepOG488, eYFP) to amino-polymersomes is an undesired

effect. Nonspecific binding of proteins has to be avoided when medical applications are the focus of the research. Nonspecific binding would lead to an undesirable, fast clearance of the polymersomes by MPS cells [38].

In Ref. [65] two papers are cited which show the reaction of NHS-esters with secondary amines [106, 107]. But sluggish reaction of secondary amines with NHS-esters was reported [106]. And in the other paper, these reactions were analyzed in anhydrous dioxane solution, which is a completely different environment as compared to aqueous buffers [107]. Because hydrolysis of NHS-esters is fast at higher pH, it is necessary that the amine have good reactivity with NHS-esters. Otherwise, hydrolysis is dominant. A great excess of NHS-linkers as compared to the amine groups could increase the number of coupling products. But coupling of NHS-linkers to polymersomes with secondary amines is perhaps not the best choice. In an unrelated product it is stated explicitly that biotin-NHS (analog to S-4FB) only reacts with primary amines, whereas the more reactive biotin-PFB (analog to PEG_4PFB) reacts with primary and secondary amines [108].

The reaction of the secondary amines on the polymersomes with NHS-esters has been tested in Ref. [65] with NHS activated Alexa Fluor 633. But again, the negative sample, which has been used to correct for nonspecific binding, was not suitable. Only nonspecific binding to 100% AB-OH polymersomes was measured. But it is possible that nonspecific binding to amino polymersomes is bigger compared to hydroxyl polymersomes. Maybe nonspecific binding even increases with the AB-NH concentration. This would result in the same linear increase in the number of fluorophores per polymersome with increasing AB-NH concentration. Negative samples for each AB-NH concentration should have been evaluated to exclude nonspecific binding from the data.

A ^{1}H-NMR spectrum of the AB-NH polymer is presented in the appendix (Fig. 31). The spectrum looks roughly the same as the previous ^{1}H-NMR spectrum of the same polymer (Fig. S3 [65]). In particular, the peaks for the piperazyl group at 2.61 ppm and 2.81 ppm are similar. Only the peak at 1.66 ppm is much bigger, but this peak could not be identified. But it can be concluded that the functional group (piperazyl) was still present. The polymer was not decomposed over time, the amino groups should have been accessible as reported [65]. The fact that it was possible to functionalize the amino-polymersomes with the PEG_4PFB linker confirms this assumption.

4.10 Biological Experiments

Although the concentration of heparin in V-DAPH could not be determined and the successful coupling of heparin to V-DAPH was not shown definitely, some biological experiments were performed. First, V-DAPH were added to cultured parasitized erythrocytes and not infected erythrocytes. As a control 1 mg/ml heparin in PBS was added to another culture plate, whereas the final concentration was 100 µg/ml, what should lead to about 90% invasion inhibition [15]. Invasion inhibition was determined after at least one full replication cycle of the parasite. But no invasion inhibition was observed with either V-DAPH or with 100 µg/ml heparin.

To check if V-SRB with a mean diameter of 80 nm have access to infected erythrocytes, the same

experiment was repeated with V-SRB (Fig. 27).

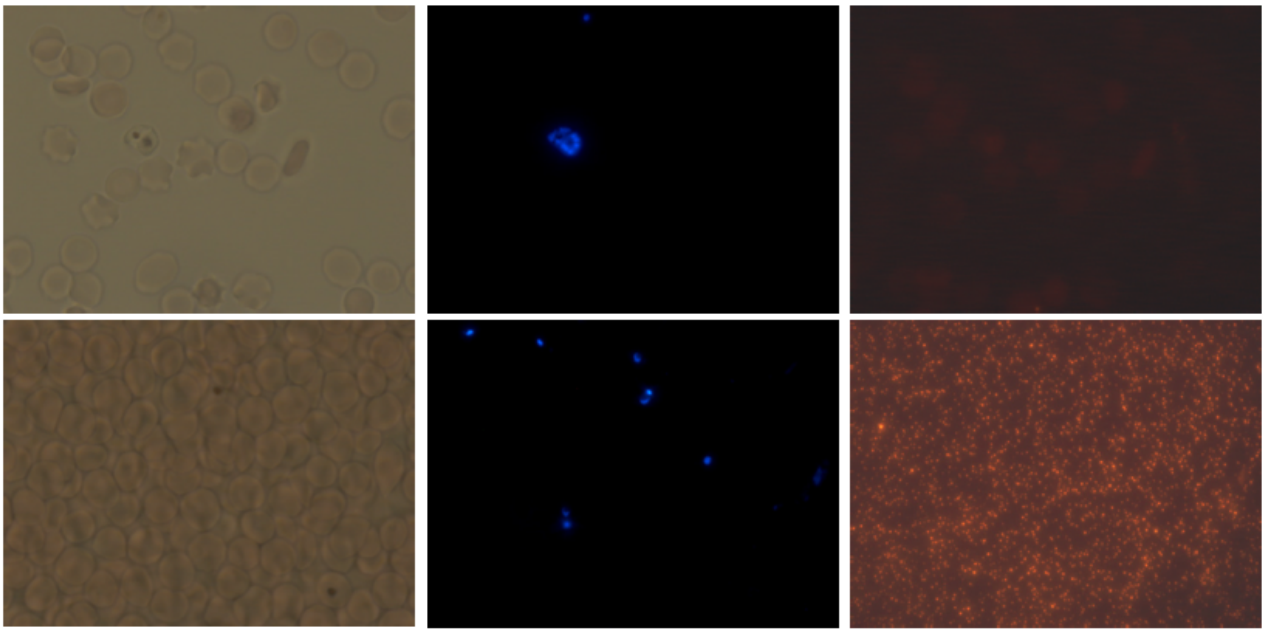

Figure 27: Blood smears after 3 days incubation of parasitized erythrocytes with V-SRB (80 nm). Left, bright field, middle DAPI staining, and right fluorescence of V-SRB. Top, after washing. Bottom, before washing.

The figure shows that infected erythrocytes did not take up 80 nm V-SRB. If V-SRBs were destroyed after the uptake, the whole infected erythrocyte should be colored faintly. But this was not observed. Because latex beads with diameters up to 80 nm can enter IEs [75], polymers which lead to 50 nm polymersomes should be evaluated in the future.

4.11 Practical Observations

Some important practical observations made during this master's thesis are presented here. First, to concentrate polymersome samples centrifugal filters (MWCO = 100 kDa, 13,400 RPM) were used. To check if polymersomes were stable enough to sustain this procedure, V-SRB were measured with FCS before and after concentration with centrifugal filters. This data showed clearly that polymersomes did not burst during concentration because no free SRB was measured. Also filtration of polymersomes through 0.45 µm pores was tested in the same way. Filtration was possible as well without destroying the polymersomes. This is necessary to get sterile samples for cell culture experiments. An unsolved problem was the determination of exact polymersome concentrations. FCS is not suitable because polymersomes approach the diameter of the confocal volume. Another problem was precipitation of the polymer. For some unknown reasons it happened sometimes that polymersomes were formed but the polymer precipitated suddenly in any next step.

5 Conclusions

Here, a new concept for the treatment of malaria was presented. Two concepts to obtain heparin-polymersome conjugates were tested in this work. Biological experiments to test the antimalarial effect did not show any invasion inhibition by heparin or heparin-polymersome conjugates. Neither the one-pot approach nor the indirect coupling via a linker system resulted clearly in the desired coupling product. On the one hand, the coupling of heparin to polymersomes might not have been successful, but time did not permit further investigation. On the other hand, the detection methods for heparin turned out not to be suitable, due to non-specific binding of proteins to amino-terminated polymersomes (V-NH) and to the linker-functionalized polymersomes (V-4FB, V-PEG4FB). This limits the use of FCS as the detection method and is highly undesirable in regard to a medical application. Furthermore, it gave rise to doubts as to whether the linker system ever worked at all for these polymersomes. But final conclusions about the usage of this linker system for polymersome surface modifications are not possible at this titme.

6 Outlook

Because the heparin-polymersome conjugates could not be produced as desired, other ways of synthesis should be examined. If the heparin concentration were in the range of the toluidine blue assay, this method would seem to be useful for the quantification of coupled heparin. But otherwise, different heparin detection methods have to be tested. Here, an attempt was made to put heparin in its natural conformation onto the already formed polymersomes. The other possibility is the synthesis of a heparin-polymer conjugate before self-assembly [47]. This changes the self-assembling properties of the polymer. Because heparin is very long and hydrophilic, most likely micelles are formed. But, for an invasion-inhibition conjugate, it is not necessary to have a hollow structure. For example, polymeric worm-like micelles have shown very long circulation times of about one week in rats [109]. This is a factor of 10 longer than for spheres.

To eliminate the anticoagulation property, partial chemical or biological degradation of heparin might be suitable. Another possibility would be the purification of heparin from the 22% that carry the specific pentasaccharide for the anticoagulation activity [47]. Or heparin analogs such as K5 polysaccharide, which has no anticoagulation properties, could be used [15].

Another interesting approach would be the design of peptidic heparin analogs that would exclusively bind to MSP1. Sulfated peptides did form stronger interactions with heparin-binding proteins than heparin itself [49, 50]. A stronger interaction would be desirable for merozoite invasion inhibition. In particular, if a peptide without any anticoagulation properties, but with MSP1 binding capacity could be found, it would open new possibilities for an anti-invasion drug. Maybe it would even be possible to construct nanostructures with these peptides, as is described for other peptides [110].

On the other hand, targeted drug delivery to IEs with polymeric carrier systems was not broadly examined until now [73]. This could be done in the future in order to test whether different artifi-

cial carriers can transport an antimalarial to IEs. Here, one very interesting experiment would be the encapsulation of heparin into a nanocontainer and the subsequent targeted delivery to IEs. If those nanocarriers are taken up by IEs, pH-sensitive polymersomes, for example, would release the heparin inside the IE, where it can bind to the merozoites before their egress from the IE. This formulation would shield the heparin from the blood stream, it would not exhibit its anticoagulation property and would have a longer circulation time. Furthermore, the dosage needed should be smaller than for free heparin and oral administration becomes perhaps possible.

Finally, the concept of invasion inhibition with functionalized polymersomes is perhaps worth consideration and trial in viral infections.

7 Acknowledgments

First of all I thank Prof. Dr. Wolfgang Meier and Prof. Dr. Hans-Peter Beck for giving me the opportunity to test this concept in their groups. For supervision and many discussions I kindly thank Martin Nussbaumer, Dr. Stefan Egli, and Dr. Sebastian Marco Rusch. Furthermore, I thank Dr. Stefan Egli for the polymers, Dr. Sebastian Marco Rusch for performing the biological experiments, Dr. Nico Bruns for help with the linker system, Gabriele Persy for TEM, Christoph Müller for providing eYFP, Patric Baumann for the columns, and Etienne Cabane and Dominik Dobrunz for help with NMR. Finally, I thank Dr. Mark Inglin for the revision of this report and my brother Tobias Najer for the design of the title page showing the concept of this work. And of course I thank all other group members for the nice atmosphere, discussions, and help.

References

[1] Pedro L Alonso, Graham Brown, Myriam Arevalo-Herrera, Fred Binka, Chetan Chitnis, Frank Collins, Ogobara K Doumbo, Brian Greenwood, B Fenton Hall, Myron M Levine, Kamini Mendis, Robert D Newman, Christopher V Plowe, Mario Henry Rodríguez, Robert Sinden, Laurence Slutsker, and Marcel Tanner. A research agenda to underpin malaria eradication. *PLoS Medicine*, 8(1):e1000406, 2011.

[2] Arjen M. Dondorp, François Nosten, Poravuth Yi, Debashish Das, Aung Phae Phyo, Joel Tarning, Khin Maung Lwin, Frederic Ariey, Warunee Hanpithakpong, Sue J. Lee, Pascal Ringwald, Kamolrat Silamut, Mallika Imwong, Kesinee Chotivanich, Pharath Lim, Trent Herdman, Sen Sam An, Shunmay Yeung, Pratap Singhasivanon, Nicholas P.J. Day, Niklas Lindegardh, Duong Socheat, and Nicholas J. White. Artemisinin resistance in plasmodium falciparum malaria. *New England Journal of Medicine*, 361(5):455–467, 2009.

[3] Stefan H. I. Kappe, Ashley M. Vaughan, Justin A. Boddey, and Alan F. Cowman. That was then but this is now: Malaria research in the time of an eradication agenda. *Science*, 328(5980):862 –866, May 2010.

[4] Rajesh Singh and James W Lillard. Nanoparticle-based targeted drug delivery. *Experimental and Molecular Pathology*, 86(3):215–223, June 2009.

[5] Alan F. Cowman and Brendan S. Crabb. Invasion of red blood cells by malaria parasites. *Cell*, 124(4):755–766, 2006.

[6] Philip Bejon, John Lusingu, Ally Olotu, Amanda Leach, Marc Lievens, Johan Vekemans, Salum Mshamu, Trudie Lang, Jayne Gould, Marie-Claude Dubois, Marie-Ange Demoitié, Jean-Francois Stallaert, Preeti Vansadia, Terrell Carter, Patricia Njuguna, Ken O. Awuondo, Anangisye Malabeja, Omar Abdul, Samwel Gesase, Neema Mturi, Chris J. Drakeley, Barbara Savarese, Tonya Villafana, W. Ripley Ballou, Joe Cohen, Eleanor M. Riley, Martha M. Lemnge, Kevin Marsh, and Lorenz von Seidlein. Efficacy of RTS,S/AS01E vaccine against malaria in children 5 to 17 months of age. *New England Journal of Medicine*, 359(24):2521–2532, 2008.

[7] A L Goodman and S J Draper. Blood-stage malaria vaccines - recent progress and future challenges. *Annals of Tropical Medicine and Parasitology*, 104(3):189–211, April 2010.

[8] Rebecca A. O'Donnell, Tania F. de Koning-Ward, Rachel A. Burt, Moses Bockarie, John C. Reeder, Alan F. Cowman, and Brendan S. Crabb. Antibodies against merozoite surface protein (Msp)-119 are a major component of the Invasion-Inhibitory response in individuals immune to malaria. *The Journal of Experimental Medicine*, 193(12):1403 –1412, June 2001.

[9] Jack S Richards and James G Beeson. The future for blood-stage vaccines against malaria. *Immunol Cell Biol*, 87(5):377–390, May 2009.

[10] Patrick Georges Cech, Thomas Aebi, Mwanajaa Shomari Abdallah, Maxmillian Mpina, Ester Barnabas Machunda, Nicole Westerfeld, Sabine Alexandra Stoffel, Rinaldo Zurbriggen, Gerd Pluschke, Marcel Tanner, Claudia Daubenberger, Blaise Genton, and Salim Abdulla. Virosome-Formulated plasmodium falciparum AMA-1 & CSP derived peptides as malaria vaccine: Randomized phase 1b trial in Semi-Immune adults & children. *PLoS ONE*, 6(7):e22273, July 2011.

[11] Tina S. Skinner, Linda S. Manning, Wayne A. Johnston, and Timothy M. E. Davis. In vitro stage-specific sensitivity of plasmodium falciparum to quinine and artemisinin drugs. *International Journal for Parasitology*, 26(5):519–525, May 1996.

[12] David T. Riglar, Dave Richard, Danny W. Wilson, Michelle J. Boyle, Chaitali Dekiwadia, Lynne Turnbull, Fiona Angrisano, Danushka S. Marapana, Kelly L. Rogers, Cynthia B. Whitchurch, James G. Beeson, Alan F. Cowman, Stuart A. Ralph, and Jake Baum. Super-Resolution dissection of coordinated events during malaria parasite invasion of the human erythrocyte. *Cell Host & Microbe*, 9(1):9–20, January 2011.

[13] Madhusudan Kadekoppala and Anthony A. Holder. Merozoite surface proteins of the malaria parasite: The MSP1 complex and the MSP7 family. *International Journal for Parasitology*, 40(10):1155–1161, August 2010.

[14] Anna M. Vogt, Gerhard Winter, Mats Wahlgren, and Dorothe Spillmann. Heparan sulphate identified on human erythrocytes: a plasmodium falciparum receptor. *Biochemical Journal*, 381(3):593, 2004.

[15] Michelle J. Boyle, Jack S. Richards, Paul R. Gilson, Wengang Chai, and James G. Beeson. Interactions with heparin-like molecules during erythrocyte invasion by plasmodium falciparum merozoites. *Blood*, 115(22):4559–4568, June 2010.

[16] Konstantinos Koussis, Chrislaine Withers-Martinez, Sharon Yeoh, Matthew Child, Fiona Hackett, Ellen Knuepfer, Luiz Juliano, Ute Woehlbier, Hermann Bujard, and Michael J Blackman. A multifunctional serine protease primes the malaria parasite for red blood cell invasion. *EMBO J*, 28(6):725–735, March 2009.

[17] Philippa K Harris, Sharon Yeoh, Anton R Dluzewski, Rebecca A O'Donnell, Chrislaine Withers-Martinez, Fiona Hackett, Lawrence H Bannister, Graham H Mitchell, and Michael J Blackman. Molecular identification of a malaria merozoite surface sheddase. *PLoS Pathogens*, 1(3), November 2005.

[18] Rebecca A. O'Donnell, Allan Saul, Alan F. Cowman, and Brendan S. Crabb. Functional conservation of the malaria vaccine antigen MSP-119across distantly related plasmodium species. *Nat Med*, 6(1):91–95, January 2000.

[19] Asli Kulane, Hans-Peter Ekre, Peter Perlmann, Lars Rombo, Mats Wahlgren, and Birgitta Wahlin. Effect of different fractions of heparin on plasmodium falciparum merozoite invasion of red blood cells in vitro. *The American Journal of Tropical Medicine and Hygiene*, 46(5):589 –594, May 1992.

[20] L Xiao, C Yang, PS Patterson, V Udhayakumar, and AA Lal. Sulfated polyanions inhibit invasion of erythrocytes by plasmodial merozoites and cytoadherence of endothelial cells to parasitized erythrocytes. *Infect. Immun.*, 64(4):1373–1378, April 1996.

[21] D L Clark, S Su, and E A Davidson. Saccharide anions as inhibitors of the malaria parasite. *Glycoconjugate Journal*, 14(4):473–479, June 1997.

[22] Yvonne Adams, Craig Freeman, Reinhard Schwartz-Albiez, Vito Ferro, Christopher R. Parish, and Katherine T. Andrews. Inhibition of plasmodium falciparum growth in vitro and adhesion to Chondroitin-4-Sulfate by the heparan sulfate mimetic PI-88 and other sulfated oligosaccharides. *Antimicrobial Agents and Chemotherapy*, 50(8):2850–2852, August 2006.

[23] H. A. Reid and P. Sucharit. Ancrod, heparin and epsilon-aminocap- roic acid in simian knowlesi malaria. *The Lancet*, 300(7787):1110–1112, November 1972.

[24] C J Hemmer, P Kern, F G Holst, P P Nawroth, and M Dietrich. Neither heparin nor acetylsalicylic acid influence the clinical course in human plasmodium falciparum malaria: a prospective randomized study. *The American Journal of Tropical Medicine and Hygiene*, 45(5):608–612, November 1991.

[25] W F Vann, M A Schmidt, B Jann, and K Jann. The structure of the capsular polysaccharide (K5 antigen) of urinary-tract-infective escherichia coli 010:K5:H4. a polymer similar to desulfo-heparin. *European Journal of Biochemistry / FEBS*, 116(2):359–364, May 1981.

[26] Alexander G Maier, Brian M Cooke, Alan F Cowman, and Leann Tilley. Malaria parasite proteins that remodel the host erythrocyte. *Nature Reviews. Microbiology*, 7(5):341–354, May 2009.

[27] Sue A. Kyes, Susan M. Kraemer, and Joseph D. Smith. Antigenic variation in plasmodium falciparum: Gene organization and regulation of the var multigene family. *Eukaryotic Cell*, 6(9):1511–1520, September 2007.

[28] Artur Scherf, Jose Juan Lopez-Rubio, and Loïc Riviere. Antigenic variation in plasmodium falciparum. *Annual Review of Microbiology*, 62:445–470, 2008.

[29] Louis H. Miller, Dror I. Baruch, Kevin Marsh, and Ogobara K. Doumbo. The pathogenic basis of malaria. *Nature*, 415(6872):673–679, February 2002.

[30] Claire L Mackintosh, James G Beeson, and Kevin Marsh. Clinical features and pathogenesis of severe malaria. *Trends in Parasitology*, 20(12):597–603, December 2004.

[31] Susan M Kraemer and Joseph D Smith. A family affair: var genes, PfEMP1 binding, and malaria disease. *Current Opinion in Microbiology*, 9(4):374–380, August 2006.

[32] J Alexandra Rowe, Antoine Claessens, Ruth A Corrigan, and Mònica Arman. Adhesion of plasmodium falciparum-infected erythrocytes to human cells: molecular mechanisms and therapeutic implications. *Expert Reviews in Molecular Medicine*, 11:e16, 2009.

[33] Anna M Vogt, Fredrik Pettersson, Kirsten Moll, Cathrine Jonsson, Johan Normark, Ulf Ribacke, Thomas G Egwang, Hans-Peter Ekre, Dorothe Spillmann, Qijun Chen, and Mats Wahlgren. Release of sequestered malaria parasites upon injection of a glycosaminoglycan. *PLoS Pathogens*, 2(9), September 2006.

[34] http://www.zoo.ox.ac.uk/group/west/StudyOrg.html. http://www.zoo.ox.ac.uk/group/west/StudyOrg.html, July 2011.

[35] Paul Horrocks, Robert A. Pinches, Srabasti J. Chakravorty, Janni Papakrivos, Zóe Christodoulou, Susan A. Kyes, Britta C. Urban, David J. P. Ferguson, and Chris I. Newbold. PfEMP1 expression is reduced on the surface of knobless plasmodium falciparum infected erythrocytes. *Journal of Cell Science*, 118(11):2507 –2518, June 2005.

[36] V Balasubramanian, Ozana Onaca, Ramona Enea, David W Hughes, and Cornelia G Palivan. Protein delivery: from conventional drug delivery carriers to polymeric nanoreactors. *Expert Opinion on Drug Delivery*, 7(1):63–78, 2010.

[37] S. Moein Moghimi, A. Christy Hunter, and J. Clifford Murray. Long-Circulating and Target-Specific nanoparticles: Theory to practice. *Pharmacological Reviews*, 53(2):283 –318, June 2001.

[38] Martin C. Woodle. Controlling liposome blood clearance by surface-grafted polymers. *Advanced Drug Delivery Reviews*, 32(1-2):139–152, June 1998.

[39] Pavel Broz, Samantha M. Benito, CheeLoong Saw, Peter Burger, Harald Heider, Matthias Pfisterer, Stephan Marsch, Wolfgang Meier, and Patrick Hunziker. Cell targeting by a generic receptor-targeted polymer nanocontainer platform. *Journal of Controlled Release*, 102(2):475–488, February 2005.

[40] Rajesh Singh, Shailesh Singh, and James W Lillard. Past, present, and future technologies for oral delivery of therapeutic proteins. *Journal of Pharmaceutical Sciences*, 97(7):2497–2523, July 2008. PMID: 17918721.

[41] Patrick Couvreur and Christine Vauthier. Nanotechnology: intelligent design to treat complex disease. *Pharmaceutical Research*, 23(7):1417–1450, July 2006.

[42] R. N. Davidson, L. DI Martino, L. Gradoni, R. Giacchino, R. Russo, G. B. Gaeta, R. Pempinello, S. Scott, F. Raimondi, A. Cascio, T. Prestileo, L. Caldeira, R. J. Wilkinson, and A. D. M. Brycestone. Liposomal amphotericin b (AmBisome) in mediterranean visceral leishmaniasis: a multi-centre trial. *QJM*, 87(2):75 –81, February 1994.

[43] C Passirani, G Barratt, J P Devissaguet, and D Labarre. Long-circulating nanoparticles bearing heparin or dextran covalently bound to poly(methyl methacrylate). *Pharmaceutical Research*, 15(7):1046–1050, July 1998.

[44] Bohdana M. Discher, You-Yeon Won, David S. Ege, James C-M. Lee, Frank S. Bates, Dennis E. Discher, and Daniel A. Hammer. Polymersomes: Tough vesicles made from diblock copolymers. *Science*, 284(5417):1143 –1146, May 1999.

[45] G. Gatti, B. Casu, G. K. Hamer, and A. S. Perlin. Studies on the conformation of heparin by 1H and 13C NMR spectroscopy. *Macromolecules*, 12(5):1001–1007, 1979.

[46] Lei Jin, Jan Pieter Abrahams, Richard Skinner, Maurice Petitou, Robert N. Pike, and Robin W. Carrell. The anticoagulant activation of antithrombin by heparin. *Proceedings of the National Academy of Sciences*, 94(26):14683 –14688, December 1997.

[47] Diana Sebök. Amphiphilic glycopolymers and glycopeptides: Properties and applications (Doctoral thesis). physical chemistry department. basel. June 2008.

[48] Ming Wang, Deqing Zhang, Guanxin Zhang, and Daoben Zhu. The convenient fluorescence turn-on detection of heparin with a silole derivative featuring an ammonium group. *Chemical Communications*, (37):4469, 2008.

[49] Heather D Maynard and Jeffrey A Hubbell. Discovery of a sulfated tetrapeptide that binds to vascular endothelial growth factor. *Acta Biomaterialia*, 1(4):451–459, July 2005.

[50] Sung Hye Kim and Kristi L. Kiick. Heparin-mimetic sulfated peptides with modulated affinities for heparin-binding peptides and growth factors. *Peptides*, 28(11):2125–2136, November 2007.

[51] http://www.rxmed.com/b.main/b2.pharmaceutical/b2.1.monographs/CPS-%20Monographs/CPS-%20%28General%20Monographs-%20H%29/HEPARIN.html. July 2011.

[52] Robert A. Baughman, Shiv C. Kapoor, Rajesh K. Agarwal, James Kisicki, Francesca Catella-Lawson, and Garret A. FitzGerald. Oral delivery of anticoagulant doses of heparin : A randomized, Double-Blind, controlled study in humans. *Circulation*, 98(16):1610 –1615, October 1998.

[53] Yuyan Jiao, Nathalie Ubrich, Monique Marchand-Arvier, Claude Vigneron, Maurice Hoffman, Thomas Lecompte, and Philippe Maincent. In vitro and in vivo evaluation of oral Heparin–Loaded polymeric nanoparticles in rabbits. *Circulation*, 105(2):230 –235, January 2002.

[54] Melissa M. Kemp and Robert J. Linhardt. Heparin-based nanoparticles. *Wiley Interdisciplinary Reviews: Nanomedicine and Nanobiotechnology*, 2(1):77–87, 2010.

[55] JM Weiler, RE Edens, RJ Linhardt, and DP Kapelanski. Heparin and modified heparin inhibit complement activation in vivo. *The Journal of Immunology*, 148(10):3210 –3215, May 1992.

[56] Sébastien Lecommandoux and Christophe Schatz. Polysaccharide-Containing block copolymers: Synthesis, properties and applications of an emerging family of glycoconjugates. *Macromolecular Rapid Communications*, 31(19):1664–1684, 2010.

[57] Shuhei Yamada and Kazuyuki Sugahara. Potential therapeutic application of chondroitin sulfate/dermatan sulfate. *Current Drug Discovery Technologies*, 5(4):289–301, December 2008.

[58] L K Hallak, D Spillmann, P L Collins, and M E Peeples. Glycosaminoglycan sulfation requirements for respiratory syncytial virus infection. *Journal of Virology*, 74(22):10508–10513, November 2000.

[59] M Antonietti and S Förster. Vesicles and liposomes: A Self-Assembly principle beyond lipids. *Advanced Materials*, 15(16):1323–1333, 2003.

[60] Dennis E. Discher and Adi Eisenberg. Polymer vesicles. *Science*, 297(5583):967 –973, 2002.

[61] Min-Hui Li and Patrick Keller. Stimuli-responsive polymer vesicles. *Soft Matter*, 5(5):927, 2009.

[62] Ozana Onaca, Ramona Enea, David W Hughes, and Wolfgang Meier. Stimuli-responsive polymersomes as nanocarriers for drug and gene delivery. *Macromolecular Bioscience*, 9(2):129–139, February 2009.

[63] Fenghua Meng, Zhiyuan Zhong, and Jan Feijen. Stimuli-Responsive polymersomes for programmed drug delivery. *Biomacromolecules*, 10(2):197–209, February 2009.

[64] Wolfgang Meier, Corinne Nardin, and Mathias Winterhalter. Reconstitution of channel proteins in (Polymerized) ABA triblock copolymer membranes. *Angewandte Chemie International Edition*, 39(24):4599–4602, 2000.

[65] Stefan Egli, Martin G. Nussbaumer, Vimalkumar Balasubramanian, Mohamed Chami, Nico Bruns, Cornelia Palivan, and Wolfgang Meier. Biocompatible functionalization of polymersome surfaces: A new approach to surface immobilization and cell targeting using polymersomes. *Journal of the American Chemical Society*, 133(12):4476–4483, March 2011.

[66] Pavel Broz, Nadav Ben-Haim, Mariusz Grzelakowski, Stephan Marsch, Wolfgang Meier, and Patrick Hunziker. Inhibition of macrophage phagocytotic activity by a receptor-targeted polymer vesicle-based drug delivery formulation of pravastatin. *Journal of Cardiovascular Pharmacology*, 51(3):246–252, March 2008.

[67] Caroline De Vocht, An Ranquin, Ronnie Willaert, Jo A. Van Ginderachter, Tamara Vanhaecke, Vera Rogiers, Wim Versées, Patrick Van Gelder, and Jan Steyaert. Assessment of stability, toxicity and immunogenicity of new polymeric nanoreactors for use in enzyme replacement therapy of MNGIE. *Journal of Controlled Release*, 137(3):246–254, August 2009.

[68] Martin C. Woodle, Charles M. Engbers, and Samuel Zalipsky. New amphipatic Polymer-Lipid conjugates forming Long-Circulating reticuloendothelial System-Evading liposomes. *Bioconjugate Chemistry*, 5(6):493–496, November 1994.

[69] Rupert Konradi, Bidhari Pidhatika, Andreas Muhlebach, and Marcus Textor. Poly-2-methyl-2-oxazoline: A peptide-like polymer for Protein-Repellent surfaces. *Langmuir*, 24(3):613–616, February 2008.

[70] A B Mathur, T O Collier, W J Kao, M Wiggins, M A Schubert, A Hiltner, and J M Anderson. In vivo biocompatibility and biostability of modified polyurethanes. *Journal of Biomedical Materials Research*, 36(2):246–257, August 1997.

[71] Paul A McCarron, Waleed M Marouf, Ryan F Donnelly, and Chris Scott. Enhanced surface attachment of protein-type targeting ligands to poly(lactide-co-glycolide) nanoparticles using variable expression of polymeric acid functionality. *Journal of Biomedical Materials Research. Part A*, 87(4):873–884, December 2008.

[72] Stefan Egli, Helmut Schlaad, Nico Bruns, and Wolfgang Meier. Functionalization of block copolymer vesicle surfaces. *Polymers*, 3(1):252–280, 2011.

[73] Nereide Stela Santos-Magalhães and Vanessa Carla Furtado Mosqueira. Nanotechnology applied to the treatment of malaria. *Advanced Drug Delivery Reviews*, 62(4-5):560–575, March 2010.

[74] B. Pouvelle, R. Spiegel, L. Hsiao, R. J. Howard, R. L. Morris, A. P. Thomas, and T. F. Taraschi. Direct access to serum macromolecules by intraerythrocytic malaria parasites. *Nature*, 353(6339):73–75, 1991.

[75] I D Goodyer, B Pouvelle, T G Schneider, D P Trelka, and T F Taraschi. Characterization of macromolecular transport pathways in malaria-infected erythrocytes. *Molecular and Biochemical Parasitology*, 87(1):13–28, July 1997.

[76] Elke S Bergmann-Leitner, Elizabeth H Duncan, and Evelina Angov. MSP-1p42-specific antibodies affect growth and development of intra-erythrocytic parasites of plasmodium falciparum. *Malaria Journal*, 8:183, 2009.

[77] Kenneth J Longmuir, Richard T Robertson, Sherry M Haynes, Janie L Baratta, and Alan J Waring. Effective targeting of liposomes to liver and hepatocytes in vivo by incorporation of a plasmodium amino acid sequence. *Pharmaceutical Research*, 23(4):759–769, April 2006.

[78] M Owais, G C Varshney, A Choudhury, S Chandra, and C M Gupta. Chloroquine encapsulated in malaria-infected erythrocyte-specific antibody-bearing liposomes effectively controls chloroquine-resistant plasmodium berghei infections in mice. *Antimicrobial Agents and Chemotherapy*, 39(1):180–184, January 1995.

[79] Patricia Urbán, Joan Estelrich, Alfred Cortés, and Xavier Fernàndez-Busquets. A nanovector with complete discrimination for targeted delivery to plasmodium falciparum-infected versus non-infected red blood cells in vitro. *Journal of Controlled Release*, 151(2):202–211, April 2011.

[80] Yashwant Gupta, Anekant Jain, and Sanjay K Jain. Transferrin-conjugated solid lipid nanoparticles for enhanced delivery of quinine dihydrochloride to the brain. *The Journal of Pharmacy and Pharmacology*, 59(7):935–940, July 2007.

[81] VC Okoye and V Bennett. Plasmodium falciparum malaria: band 3 as a possible receptor during invasion of human erythrocytes. *Science*, 227(4683):169 –171, January 1985.

[82] http://www.nanoviricides.com/. July 2011.

[83] Alexandra Graff, Marc Sauer, Patrick Van Gelder, and Wolfgang Meier. Virus-assisted loading of polymer nanocontainer. *Proceedings of the National Academy of Sciences*, 99(8):5064 –5068, April 2002.

[84] P Jani, G W Halbert, J Langridge, and A T Florence. The uptake and translocation of latex nanospheres and microspheres after oral administration to rats. *The Journal of Pharmacy and Pharmacology*, 41(12):809–812, December 1989.

[85] Nico Bruns, Katarzyna Pustelny, Lisa Bergeron, Timothy Whitehead, and Douglas Clark. Mechanical nanosensor based on FRET within a thermosome: Damage-Reporting polymeric materials. *Angewandte Chemie International Edition*, 48(31):5666–5669, 2009.

[86] Greg F. Walker, Carolin Fella, Jaroslav Pelisek, Julia Fahrmeir, Sabine Boeckle, Manfred Ogris, and Ernst Wagner. Toward synthetic viruses: Endosomal pH-Triggered deshielding of targeted polyplexes greatly enhances gene transfer in vitro and in vivo. *Mol Ther*, 11(3):418–425, March 2005.

[87] V. D. Nadkarni, A. Pervin, and R. J. Linhardt. Directional immobilization of heparin onto beaded supports. *Analytical Biochemistry*, 222(1):59–67, October 1994.

[88] Jia Duo and Julie A. Stenken. Heparin-immobilized microspheres for the capture of cytokines. *Analytical and Bioanalytical Chemistry*, 399(2):773–782, 2010.

[89] Shinya Sato, Takeshi Sakamoto, Etsuko Miyazawa, and Yasuo Kikugawa. One-pot reductive amination of aldehydes and ketones with [alpha]-picoline-borane in methanol, in water, and in neat conditions. *Tetrahedron*, 60(36):7899–7906, August 2004.

[90] F. C. MacIntosh. A colorimetric method for the standardization of heparin preparations. *Biochemical Journal*, 35(7):776–782, July 1941.

[91] P. K. Smith, A. K. Mallia, and G. T. Hermanson. Colorimetric method for the assay of heparin content in immobilized heparin preparations. *Analytical Biochemistry*, 109(2):466–473, December 1980.

[92] Douglas Magde, Elliot Elson, and W. W. Webb. Thermodynamic fluctuations in a reacting System-Measurement by fluorescence correlation spectroscopy. *Physical Review Letters*, 29(11):705, 1972.

[93] W Trager and J B Jensen. Human malaria parasites in continuous culture. *Science (New York, N.Y.)*, 193(4254):673–675, August 1976.

[94] Adrian Najer. Determination of the diffusion coefficient of fluorescently labeled amphiphilic triblock copolymers in giant unilamellar polymeric vesicle membranes by Z-Scan fluorescence correlation spectroscopy (FCS) (Unpublished project work). physical chemistry department. basel. February 2010.

[95] Ruoyu Zhan, Zhen Fang, and Bin Liu. Naked-eye detection and quantification of heparin in serum with a cationic polythiophene. *Analytical Chemistry*, 82(4):1326–1333, February 2010.

[96] Yuya Egawa, Ryosuke Hayashida, Toshinobu Seki, and Jun ichi Anzai. Fluorometric determination of heparin based on self-quenching of fluorescein-labeled protamine. *Talanta*, 76(4):736–741, August 2008.

[97] C. B. Müller, A. Loman, V. Pacheco, F. Koberling, D. Willbold, W. Richtering, and J. Enderlein. Precise measurement of diffusion by multi-color dual-focus fluorescence correlation spectroscopy. *EPL (Europhysics Letters)*, 83(4):46001, 2008.

[98] http://www.wcaslab.com/tech/heparin_nmr.htm. July 2011.

[99] D R Ferro, A Provasoli, M Ragazzi, B Casu, G Torri, V Bossennec, B Perly, P Sinaÿ, M Petitou, and J Choay. Conformer populations of l-iduronic acid residues in glycosaminoglycan sequences. *Carbohydrate Research*, 195(2):157–167, January 1990.

[100] Solulink. S-HyNic bioconjugation technical manual. california. 2009.

[101] Greg T. Hermanson. *Bioconjugate Techniques*. Academic Press, 2nd revised edition (REV). edition, May 2008.

[102] HydraLink. Superior technology for bioconjugations and immobilizations. 2009.

[103] Martin G. Nussbaumer. Conjugation of antibodies to polymer vesicles for targeted drug delivery purposes (Unpublished master's thesis). physical chemistry department. basel. June 2010.

[104] Bryan Holtz, Yini Wang, Xiao-Yang Zhu, and Athena Guo. Denaturing and refolding of protein molecules on surfaces. *Proteomics*, 7(11):1771–1774, June 2007.

[105] Shelley R McRae, Christopher L Brown, and Gillian R Bushell. Rapid purification of EGFP, EYFP, and ECFP with high yield and purity. *Protein Expression and Purification*, 41(1):121–127, May 2005.

[106] Hermann J. Gruber, Gerald Kada, Bernt Pragl, Christian Riener, Christoph D. Hahn, Gregory S. Harms, Werner Ahrer, Thomas G. Dax, Karin Hohenthanner, and Hans-Günther Knaus. Preparation of Thiol-Reactive cy5 derivatives from commercial cy5 succinimidyl ester†. *Bioconjugate Chemistry*, 11(2):161–166, March 2000.

[107] Gary W. Cline and Samir B. Hanna. The aminolysis of n-hydroxysuccinimide esters. a structure-reactivity study. *Journal of the American Chemical Society*, 109(10):3087–3091, May 1987.

[108] http://www.piercenet.com/browse.cfm?fldID=01030911. July 2011.

[109] Yan Geng, Paul Dalhaimer, Shenshen Cai, Richard Tsai, Manorama Tewari, Tamara Minko, and Dennis E. Discher. Shape effects of filaments versus spherical particles in flow and drug delivery. *Nat Nano*, 2(4):249–255, April 2007.

[110] Dirk de Bruyn Ouboter, Thomas B. Schuster, Alexandre Mantion, and Wolfgang Meier. Hierarchical organization of purely peptidic amphiphiles into peptide beads. *The Journal of Physical Chemistry C*, 115(30):14583–14590, 2011.

Appendix

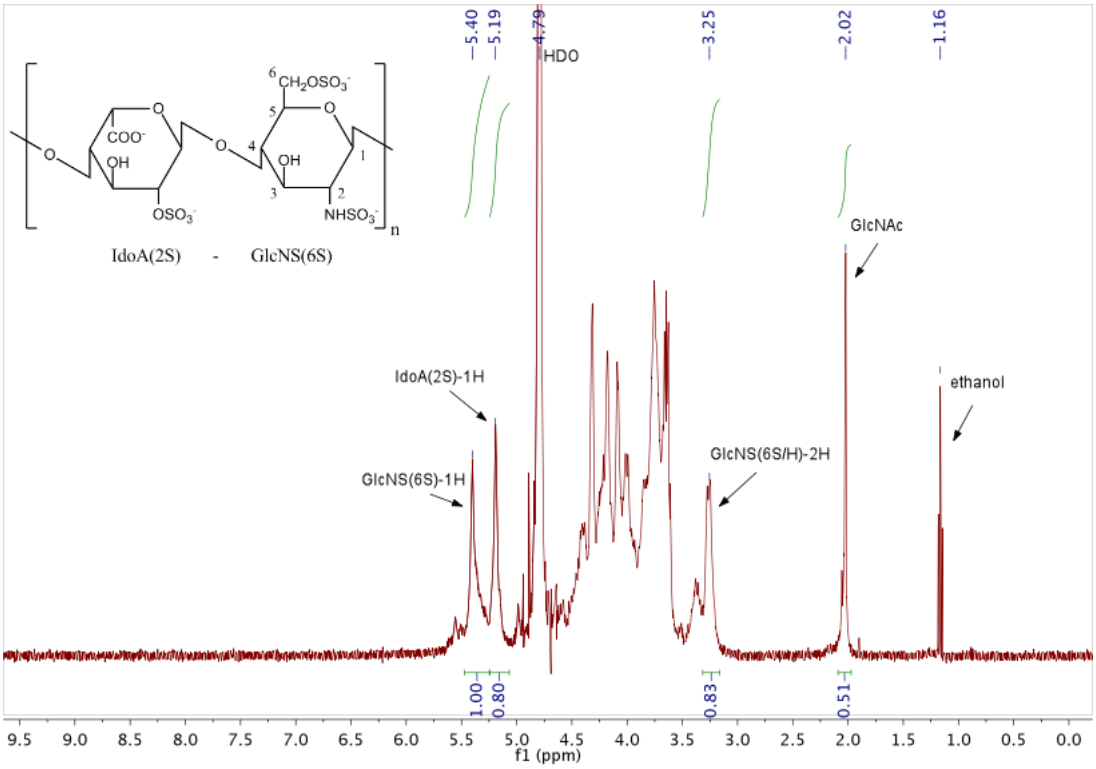

Figure 28: ^{1}H-NMR spectrum of 13 mg LMWH in 0.6 ml D_20

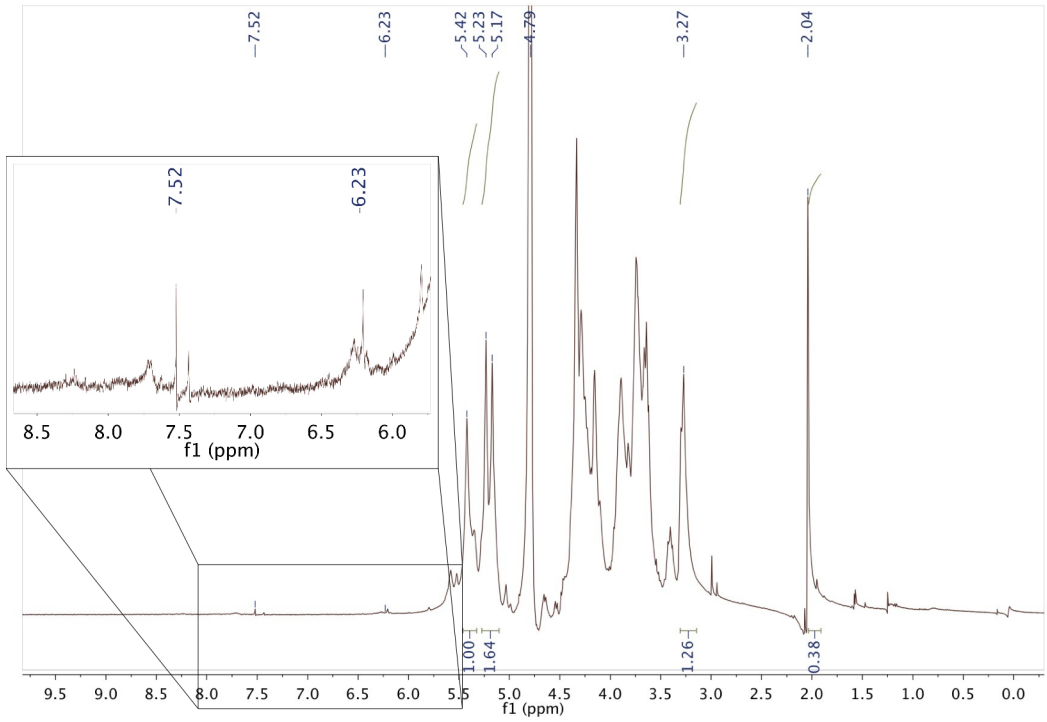

Figure 29: ^{1}H-NMR spectrum of 22 mg DAPH in 0.5 ml D_20

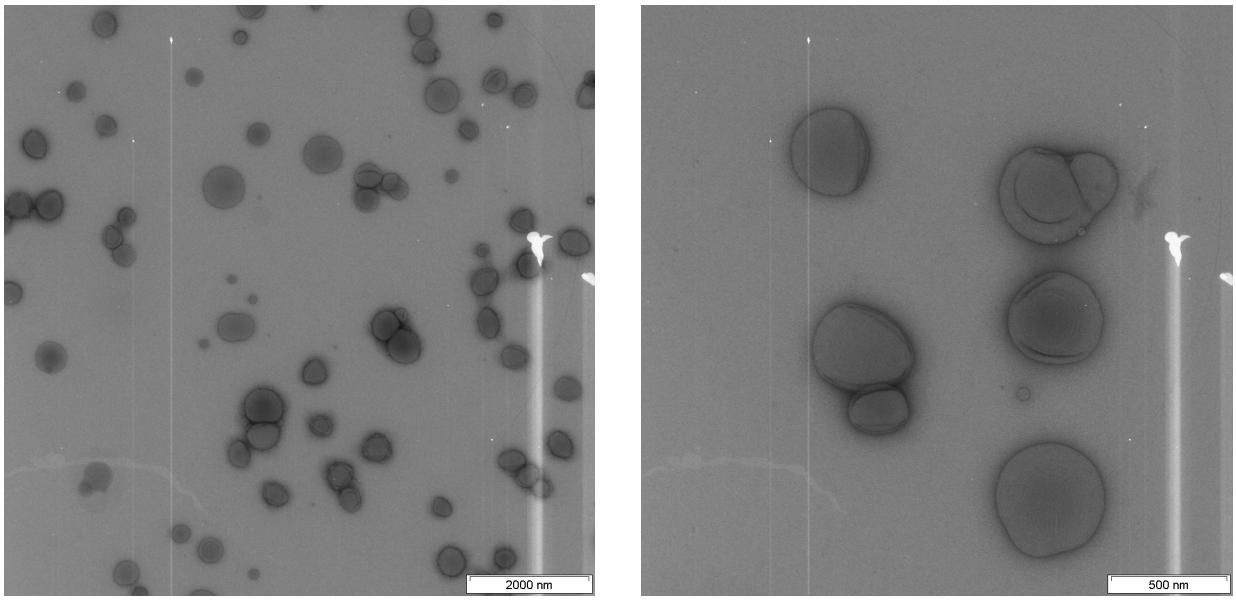

Figure 30: TEM pictures of heparin-polymersome conjugates after purification by dialysis.

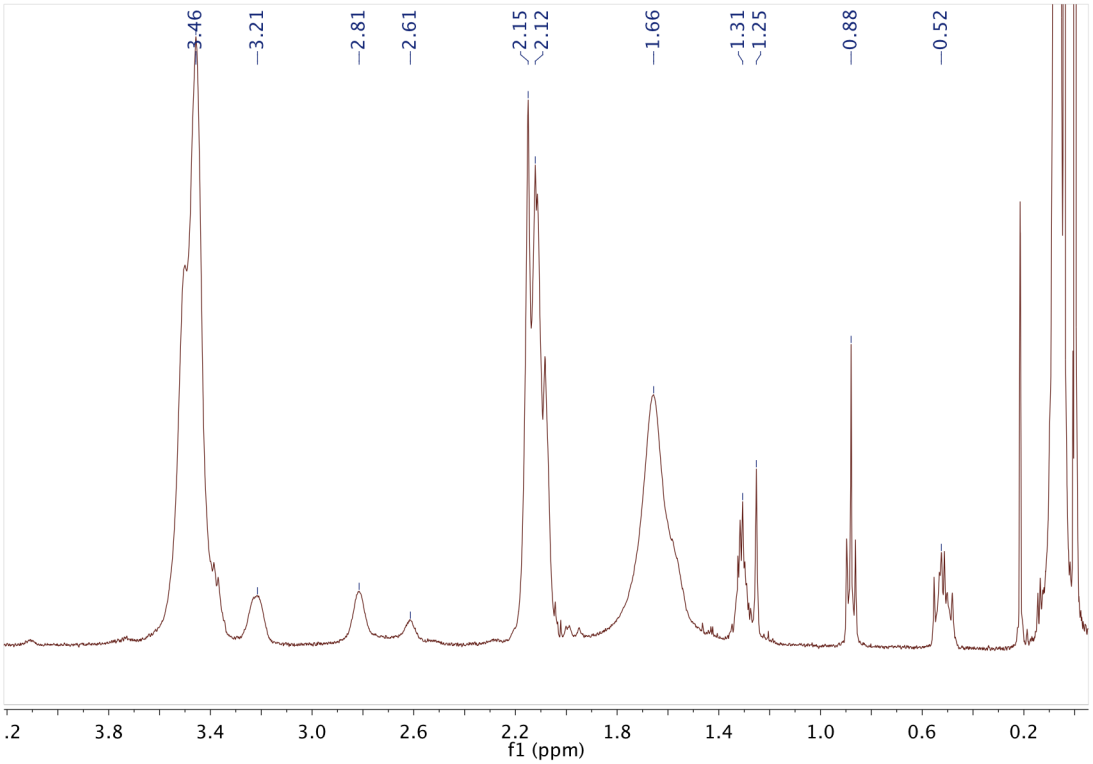

Figure 31: ^{1}H-NMR spectrum of 10 mg AB-NH in 0.5 ml $CDCl_3$.

Formular drucken

Philosophisch-Naturwissenschaftliche Fakultät
der Universität Basel
Dekanat

Erklärung zur wissenschaftlichen Redlichkeit
(beinhaltet Erklärung zu Plagiat und Betrug)

(bitte ankreuzen)
☐ Bachelorarbeit
☒ Masterarbeit

Titel der Arbeit *(Druckschrift)*:

Heparin-Polymersome Conjugates to Fool Plasmodium Merozoites

Name, Vorname *(Druckschrift)*: Adrian Najer

Matrikelnummer: 06-068-324

Hiermit erkläre ich, dass mir bei der Abfassung dieser Arbeit nur die darin angegebene Hilfe zuteil wurde und dass ich sie nur mit den in der Arbeit angegebenen Hilfsmitteln verfasst habe.

Ich habe sämtliche verwendeten Quellen erwähnt und gemäss anerkannten wissenschaftlichen Regeln zitiert.

Diese Erklärung wird ergänzt durch eine separat abgeschlossene Vereinbarung bezüglich der Veröffentlichung oder öffentlichen Zugänglichkeit dieser Arbeit.

☒ ja ☐ nein

Ort, Datum: Basel, 30.07.11

Unterschrift: 

Dieses Blatt ist in die Bachelor-, resp. Masterarbeit einzufügen.